Dust coatings on basaltic rocks and implications for thermal infrared spectroscopy of Mars

Jeffrey R. Johnson
Branch of Astrogeology, U.S. Geological Survey, Flagstaff, Arizona, USA

Philip R. Christensen
Department of Geology, Arizona State University, Tempe, Arizona, USA

Paul G. Lucey
Hawaii Institute for Geology and Planetology, University of Hawaii at Manoa, Honolulu, Hawaii, USA

Received 2 October 2000; revised 6 July 2001; accepted 12 October 2001; published 5 June 2002.

[1] Thin coatings of atmospherically deposited dust can mask the spectral characteristics of underlying surfaces on Mars from the visible to thermal infrared wavelengths, making identification of substrate and coating mineralogy difficult from lander and orbiter spectrometer data. To study the spectral effects of dust coatings, we acquired thermal emission and hemispherical reflectance spectra (5–25 μm; 2000–400 cm^{-1}) of basaltic andesite coated with different thicknesses of air fall-deposited palagonitic soils, fine-grained ceramic clay powders, and terrestrial loess. The results show that thin coatings (10–20 μm) reduce the spectral contrast of the rock substrate substantially, consistent with previous work. This contrast reduction continues linearly with increasing coating thickness until a "saturation thickness" is reached, after which little further change is observed. The saturation thickness of the spectrally flat palagonite coatings is ~100–120 μm, whereas that for coatings with higher spectral contrast is only ~50–75 μm. Spectral differences among coated and uncoated samples correlate with measured coating thicknesses in a quadratic manner, whereas correlations with estimated surface area coverage are better fit by linear functions. Linear mixture modeling of coated samples using the rock substrate and coating materials as end-members is also consistent with their measured coating thicknesses and areal coverage. A comparison of ratios of Thermal Emission Spectrometer (TES) spectra of dark and bright intracrater and windstreak deposits associated with Radau crater suggests that the dark windstreak material may be coated with as much as 90% areal coverage of palagonitic dust. The data presented here also will help improve interpretations of upcoming mini-TES and Thermal Emission Imaging System (THEMIS) observations of coated Mars surface materials. *INDEX TERMS:* 6225 Planetology: Solar System Objects: Mars; 3934 Mineral Physics: Optical, infrared, and Raman spectroscopy; 5470 Planetology: Solid Surface Planets: Surface materials and properties; 5464 Planetology: Solid Surface Planets: Remote sensing; *KEYWORDS:* Spectra, thermal infrared; coatings; remote sensing; Mars; spectra, thermal emission

1. Introduction

[2] The masking effect of aeolian dust coatings on rock and soil surfaces hampers remote-sensing investigations in visible to thermal infrared wavelengths on both the Earth and Mars. Visible/near-IR spectroscopy from the Mars Pathfinder and Viking landers and the X-ray mode of the Pathfinder alpha proton X-ray spectrometer (APXS) suggested that soil-like coatings are present on most surfaces at these landing sites and may be responsible in part for the observed paucity of significant rock and soil spectral variations [*Arvidson et al.*, 1989a, 1989b; *Guinness et al.*, 1997; *Smith et al.*, 1997; *McSween et al.*, 1999; *Bell et al.*, 2000; *Rieder et al.*, 1997; *Crisp*, 1998]. In the thermal infrared (TIR), relatively thin silicate coatings (<50 μm) can obscure the spectral character of underlying materials and significantly reduce spectral contrast, making mineral identification more difficult compared to dust-free surfaces [*Van Tassel and Salisbury*, 1964; *Crisp and Bartholomew*, 1992; *Salisbury et al.*, 1994; *Johnson et al.*, 1998; *Cooper and Mustard*, 1999]. Discriminating spectral features in remotely sensed data sets related to such fine-particle coatings from those attributable to the underlying rock is difficult. Previous attempts relied on comparisons of "clean" and variously weathered or dust-coated regions to understand and compensate for the spectral effects of coatings [*Mustard and Sunshine*, 1995; *Moersch et al.*, 1997].

[3] TIR spectroscopy of the Martian surface can determine the composition and distribution of minerals, rocks, soils, and ices [*Sinton and Strong*, 1960; *Hanel et al.*, 1972, 1992; *Christensen et al.*, 1992, 1998, 2000a, 2000b, 2000c; *Bandfield et al.*, 2000a, 2000b; *Kieffer et al.*, 2000]. This information helps constrain the formational environments of surface materials and improves our knowledge of the styles, extent, and evolution of geochemical weathering and climate on Mars. Identification of minerals indicative of specific igneous rock types can help focus studies of Martian volcanism and crustal petrogenesis related to planetary geological evolution [e.g., *Hanel et al.*, 1972; *Christensen et al.*, 1992; *McSween et al.*, 1999; *Bandfield et al.*, 2000a]. Detection of salts or alteration minerals (e.g., carbonates, sulfates, ferric oxides, clays) might be indicative of regions where past aqueous or hydrothermal activity resulting from different climatic or crustal

0148-0227/02/2000JE001405$09.00

thermal conditions led to environments that would provide candidate sites for exobiologic studies [e.g., *Farmer and Des Marais*, 1999].

[4] Significant progress has been made in modeling the effects of atmospheric dust, surface temperatures, particle size, and the deconvolution of mineral mixtures necessary to interpret remotely sensed TIR spectra of Mars [e.g., *Moersch and Christensen*, 1995; *Mustard and Hays*, 1997; *Ramsey and Christensen*, 1998; *Christensen et al.*, 1998, 2000a, 2000b, 2000c; *Bandfield et al.*, 2000b; *Smith et al.*, 2000; *Hamilton and Christensen*, 2000]. However, the effect of dust coatings on rock surfaces is an additional complicating factor that must be better understood to identify more precisely the mineralogy and chemical compositions and variability of rocks and soils on Mars.

[5] Using laboratory directional hemispherical reflectance and emission spectroscopy (5–25 μm; 2000–400 cm^{-1}), we investigate here the spectral effects of fine-grained coatings of variable thickness deposited on basaltic andesite rock substrates. These effects are relevant to interpretation of TIR spectra of the Martian surface provided by the Thermal Emission Spectrometer (TES) aboard Mars Global Surveyor (MGS) [*Christensen et al.*, 1992, 1998, 2001], to future Mars spectra from the mini-TES instrument [*Squyres et al.*, 1999] and the Thermal Emission Imaging System (THEMIS) [*Christensen et al.*, 1999], as well as to TIR images of Earth provided by instruments such as the Advanced Spaceborne Thermal Emission and Reflection Radiometer (ASTER) [e.g., *Ramsey and Lancaster*, 1998]. These types of laboratory measurements are more directly comparable to remotely sensed data such as those from TES, as opposed to transmission, absorption, or biconical reflectance spectra, which do not measure as precisely the total radiation detected by TES-like instruments. The spectra presented here provide additional end-member spectra to linear mixing models [e.g., *Thomson and Salisbury*, 1993; *Ramsey and Christensen*, 1998; *Feely and Christensen*, 1999] that could be used to identify and determine mineral abundances from TES spectra of both the dust coating and the obscured substrate. The data also will contribute much-needed laboratory spectra to constrain models of layered or coated surfaces [e.g., *Emslie and Aronson*, 1973; *Aronson and Emslie*, 1973, 1975; *Henderson and Jakosky*, 1997; *Johnson and Grundy*, 2001].

[6] Large amounts of dust (<40 μm particles) can be moved during major dust storms on Mars. *Christensen* [1986] concluded that global storms could deposit as much as ~250 μm per year throughout geologic time in the equatorial region. *White et al.* [1997] suggested that dust coatings are more easily lifted from rougher rock surfaces than from smooth soils, implying that the fine-particle coatings on rock surfaces could be relatively transitory deposits. Narrow-angle Mars Orbiter Camera (MOC) images have revealed surfaces that are dark compared to their immediate surroundings which are interpreted to represent areas where dust coatings have been scoured by dust devils and small landslides, demonstrating current dust mobilization [*Edgett and Malin*, 2000; *Sullivan et al.*, 2000; *Metzger et al.*, 1999]. The ability to quantitatively track regional dust coatings across Mars from TES spectra would improve mineralogical analysis of both the dust and underlying materials. It would also contribute additional constraints to models of wind dynamics, aeolian activity, and global circulation models [e.g., *Haberle*, 1999; *Rafkin et al.*, 2001].

2. Background

[7] The spectral effects of fine-grained particles have been studied extensively in the TIR both theoretically and in the laboratory using a variety of materials in absorbance [e.g., *Pecharroman and Igelsias*, 1996], reflectance [e.g., *Salisbury et al.*, 1991b; *Christy et al.*, 1993; *Salisbury*, 1993; *Mustard and Hays*, 1997; *Cooper and Mustard*, 1999], and emission [*Moersch and Christensen*, 1995; *Henderson and Jakosky*, 1997]. Most silicate mineral absorption bands exhibit a decrease in spectral contrast with decreasing particle size in the >8 μm (1250 cm^{-1}) spectral region owing to the increased number of surface scattering facets per unit volume. Conversely, spectral contrast tends to increase with decreasing particle size at wavelengths <8 μm because of volume scattering [*Salisbury et al.*, 1991b; *Salisbury*, 1993]. Carbonates and sulfates tend to exhibit the opposite trends [e.g., *Hunt and Vincent*, 1968; *Salisbury et al.*, 1987; *Salisbury and Wald*, 1992].

[8] We concentrate in this paper on dust coatings on rocks rather than weathered surfaces such as desert varnish found on rocks on Earth. Such thin film layers on substrates have received as much attention for engineering and industrial purposes [e.g., *Xu and Shen*, 1992; *Ho and Ma*, 1997] as for geologic surfaces [e.g., *Emslie and Aronson*, 1973; *Hapke*, 1993]. Weathered/varnished surfaces in particular already have been studied extensively in the visible/near-IR and TIR for their relevance to terrestrial and Martian spectral interpretation [*Roush*, 1982; *Christensen and Harrison*, 1993; *Rivard et al.*, 1993; *Younis et al.*, 1997; *Eby et al.*, 1998; *Shelfer and Morris*, 1998; *Shepard and Arvidson*, 1999]. Thin films of terrestrial varnish reduce spectral contrast of the substrate rock in a manner somewhat similar to dust coatings. However, lower porosity surfaces (such as varnish films or indurated crusts) have greater spectral contrast than porous surfaces (such as air fall-deposited dust coatings) in the reststrahlen region [*Salisbury et al.*, 1991b; *Johnson et al.*, 1998; *Cooper and Mustard*, 1999], which could provide a means to differentiate between dusted and varnished surfaces.

[9] Previous laboratory investigations of the spectral effects of dust coatings have dominantly exploited the visible/near-IR to replicate the brightening effects of dust deposition in these wavelengths [cf. *Singer and Blake*, 1983]. The methods of deposition and thickness measurement have varied with each study. *Singer and Roush* [1983] deposited palagonitic soil onto a basalt substrate using differential settling in a methanol suspension and measured the coating thickness using thin sections of epoxy-coated samples. *Wells et al.* [1984] and *Thomas et al.* [1984] deposited fine-grained (<5 μm) palagonitic soil onto larger size fractions of volcanic soil and basalt powders using an enclosed cylinder in which the palagonite particles settled onto the samples after being elevated by blasts of compressed air. By estimating the coating density and calculating its mass per unit area, they computed a coating thickness. *Fischer and Pieters* [1993] and *Hiroi and Pieters* [1992] deposited powders (<25 μm) onto a basaltic substrate using the differential settling method in ethanol and measured coating thickness directly using a vertically calibrated microscope. *Lindstrom and Lindstrom* [1998] deposited the JSC-1 Martian regolith simulant [*Allen et al.*, 1998] onto several rock type substrates and estimated the coating thickness using the mass/area method.

[10] *Henry* [1948] obtained TIR transmission spectra of quartz and zinc sulfate powder films deposited onto rocksalt disks using a differential suspension method and noted a reduction in spectral contrast with increasing powder thickness. *Van Tassel and Salisbury* [1964] and *Hunt and Logan* [1972] noticed similar effects in thermal emission spectra of fine-grained minerals of variable deposited thickness. *Crisp and Bartholomew* [1992] obtained biconical TIR reflectance measurements of palagonite coatings (<20 μm Pahala ash) hand-sifted onto basalt and quartzite substrates. This method resulted in clumps of particles of highly variable thickness covering the substrate, which they measured using a calibrated microscope to obtain an average thickness. They found that the reflectance of coated rocks is linearly related to the surface area coverage and thickness of the coatings and that a small amount of palagonite can reduce the spectral contrast of the substrate significantly. However, their use of biconical reflectance is not directly applicable to emittance obtained from TES-like instruments, as it undersamples the diffusely and specularly scat-

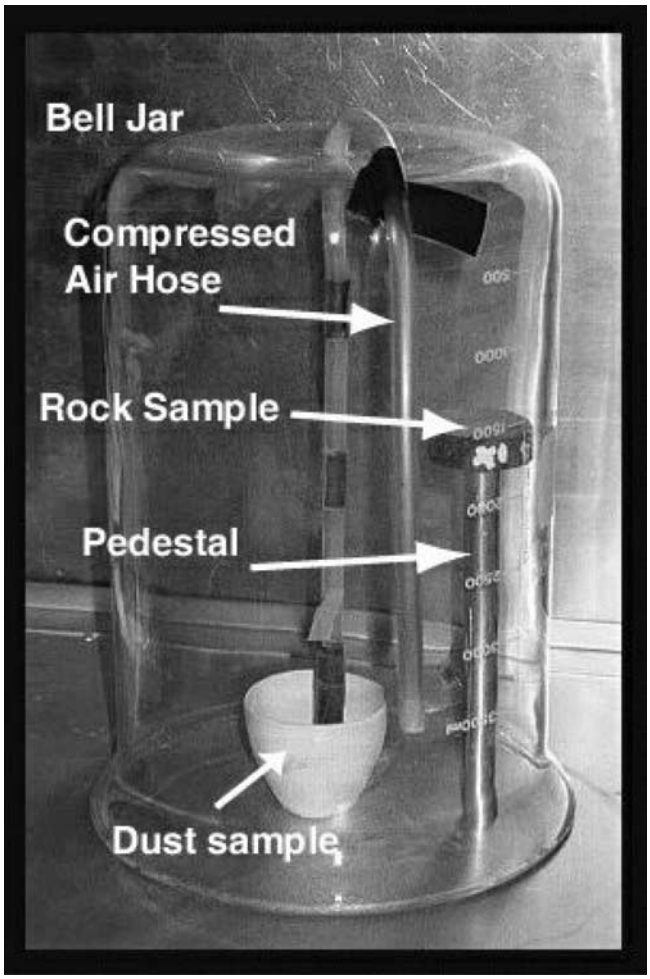

Figure 1. Dust deposition apparatus used in this study. A 4 liter bell jar was placed over a cup containing the dust sample. The dust was elevated by bursts of compressed air delivered to the sample cup via an air hose. The rock sample to be coated was placed on a pedestal above the cup to reduce deposition of large particle aggregates.

tered radiation by a factor of ~2.5 [*Salisbury*, 1993]. It is also subject to low incidence angle grazing of the illuminating radiation, which can have a significant effect on the spectra of fine particles because of forward scattering, particularly in the region near the mineralogically diagnostic Christiansen feature (~8 μm; 1250 cm^{-1}) [*Salisbury*, 1993; *Salisbury et al.*, 1991a, 1991b]. These problems are resolved by using an integrating sphere to obtain directional hemispherical reflectance [e.g., *Salisbury and Walter*, 1989; *Salisbury et al.*, 1991a, 1991b, 1997; *Johnson et al.*, 1998] and/or an emission spectrometer [e.g., *Lyon*, 1963, 1964; *Conel*, 1969; *Ruff et al.*, 1997; *Christensen et al.*, 2000b] as is done in this work.

3. Methodology

3.1. Samples

[11] The substrate used in these experiments was a basaltic andesite from the SP Mountain Flow, Arizona [*Ulrich*, 1987], that exhibited little vesicularity. A basaltic andesite was chosen to represent the dominant igneous rock type thought to comprise much of the Martian bedrock as interpreted from analysis of APXS and TES data [e.g., *McSween et al.*, 1999; *Bandfield et al.*, 2000b]. The sample was cored, cut into 3.8 cm diameter disks, and polished using 400-grit (~22 μm particles) [cf. *Fischer and Pieters*, 1993].

[12] Five coating materials were used in this work: (1) the Mars regolith simulant JSC-1 (a palagonitic soil [*Allen et al.*, 1998]) wet-sieved to a grain size fraction <45 μm); (2) a palagonitic soil collected from South Point on the island of Hawaii (Pahala ash [cf. *Crisp and Bartholomew*, 1992]), wet-sieved to <53 μm; (3) a loess sample from Ellensburg, Washington, wet-sieved to <53 μm; (4) the ceramic clay powder "Redart"; and (5) the ceramic ball clay powder "OM-4," both with grains sizes <30 μm. Palagonites describe a large class of poorly crystalline, variably weathered basaltic glasses. Their visible/near-infrared spectral properties are analogous to those observed for Mars [e.g., *Bell*, 1996]. They tend to have subtle, high-emissivity (low-reflectance) spectral features in the TIR [cf. *Roush et al.*, 1991; *Roush and Bell*, 1994; *Roush and Orenberg*, 1994; *Roush et al.*, 1994; *Hamilton et al.*, 2001] that mask underlying surfaces well. The loess and ceramic clays were used to provide nonbasaltic materials that exhibit different and stronger spectral features in the TIR compared to the JSC-1 and Pahala ash coatings [cf. *Salisbury et al.*, 1991b].

3.2. Dust Deposition

[13] In order to mimic the air fall deposition of dust onto rocks on Mars, the simple deposition technique of *Wells et al.* [1984] was used to coat the basaltic andesite samples (Figure 1). The coating material was placed in a cup in an enclosed bell jar. The coating was elevated by a pulse of compressed air and allowed to settle onto the rock sample, which was placed on a pedestal above the cup to limit deposition of large dust aggregates. The amount of material deposited on the sample was varied by placing different amounts of dust in the sample cup. This air fall deposition method is preferable to suspension/settling techniques because cracked surfaces can result after the drying process. These surfaces do not imitate air fall-deposited surfaces well and introduce unwanted textural effects that can influence the TIR spectral response.

[14] The deposition was conducted on-site at both spectrometer sample preparation facilities directly prior to acquisition of TIR spectra. Transport of predeposited samples would not have preserved the desired air fall surface textures, nor would have affixing the samples with an infrared-transparent epoxy. Samples were prepared at thicknesses from 0 to 150+ μm to cover the range over which fine-grained coatings have been estimated to obscure the spectral signature of the substrate [e.g., *Crisp and Bartholomew*, 1992; *Christensen and Harrison*, 1993].

[15] Coating thicknesses were determined using a vertically calibrated microscope to measure the focus distances between the substrate and the coating at 25 locations on the sample within the region sampled by the spectrometers. We chose this method over the mass/area method [e.g., *Wells et al.*, 1984] because the thickness can be determined without requiring estimates of deposit density. The standard deviations on our measurements of coating thickness were not due to the precision of the microscope stage (1 μm) but rather due to the partial clumping of small particles into larger aggregates (~10–50 μm) that was observed in all dust deposition experiments [cf. *Lyon*, 1964; *Crisp and Bartholomew*, 1992]. Such aggregate particles likely formed because of a combination of electrostatic and hygroscopic effects, resulting in an uneven thickness distribution of deposited particles. Laboratory experiments of dust aggregation and deposition also have shown that such "sticking" behavior is common for small particles, especially those with irregular shapes [*Blum and Wurm*, 2000; *Banerjee and Mazumder*, 2000]. We believe that air fall deposition on Mars likely results in aggregates of particles as well. Although particulates in the Martian atmosphere have been modeled to be ~1–2 μm [e.g., *Clancy and Lee*, 1991; *Tomasko et al.*, 1999], estimates of surface dust grain sizes from the Sojourner rover electrostatic charging and wheel track experiments were 20–40 μm or less [*Ferguson et al.*, 1999; *Moore et al.*, 1999].

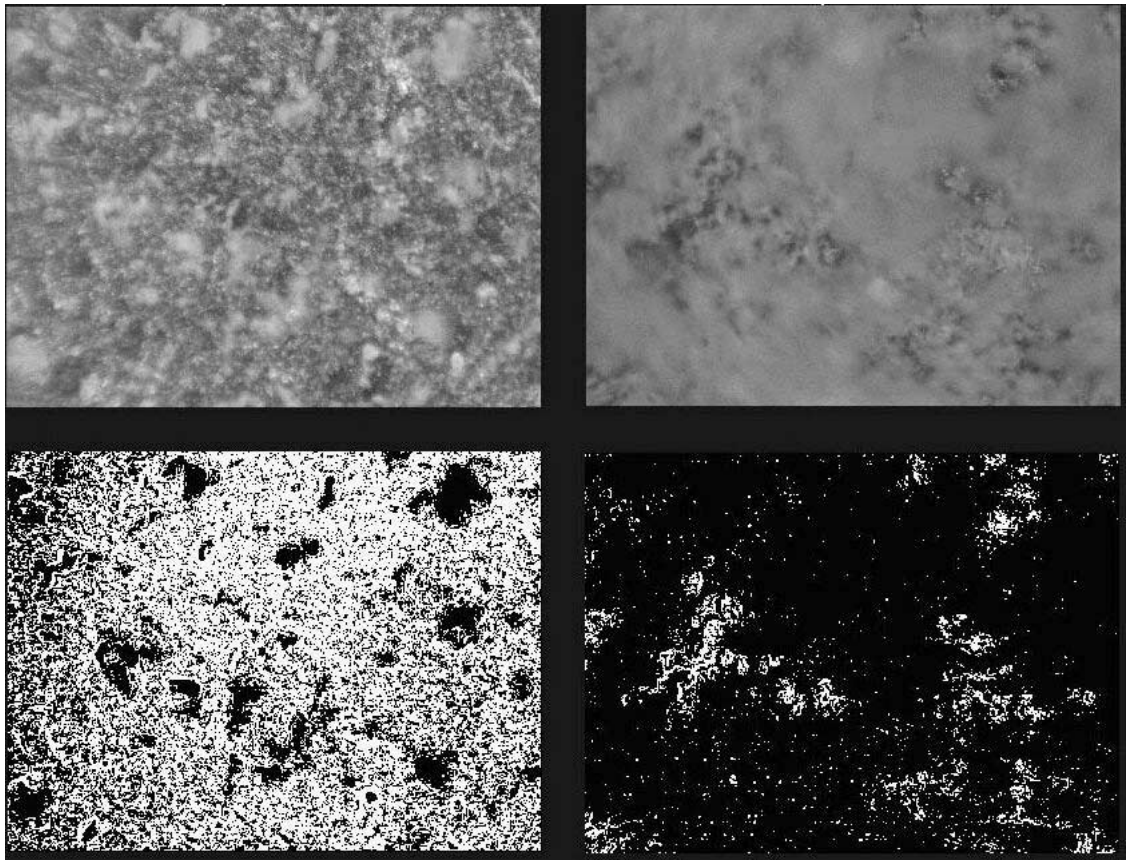

Figure 2. (top) Photomicrographs of (left) thin (19 ± 8 μm) and (right) thick (106 ± 34 μm) coatings of JSC-1 soil deposited on SP basaltic andesite samples, with the focus at the substrate. (bottom) Areal distribution maps of coated samples (rock substrate, white; JSC-1 particles, black) computed using a variance operator on each image (thin coating, 28 ± 7% coverage; thick coating, 94 ± 1%). Field of view is ~630 μm.

[16] Digital photomicrographs of the coated samples obtained with the focus at the substrate level are shown in Figure 2 for samples coated with thin (19 ± 8 μm) and thick (106 ± 34 μm) coatings of JSC-1 soil. Such images also were used to estimate the areal coverage of a given dust deposit by using a variance operator on the digital image [e.g., *Jähne*, 1995] to determine those regions that were in focus (high-variance regions, i.e., uncoated) versus those out of focus (low-variance regions, i.e., coated). Masks were created from the variance images using an empirically determined threshold value that provided a good match of the observed distribution of grains and grain aggregates. The bottom images in Figure 2 show examples of the resulting "maps" of deposited grains (in black) and uncoated substrate (in white) for a thin and thick JSC-1 coating. Using these maps, percentages of areal coverage were computed at two different locations per sample for comparison to the thicknesses estimated using the microscope.

3.3. Spectroscopy

[17] Fourier transform infrared (FTIR) spectrometers at the University of Hawaii (UH) and Arizona State University (ASU) were used to obtain directional hemispherical reflectance and emissivity spectra, respectively. Acquisition of spectra using both UH and ASU instruments permitted comparison of reflectance and emission techniques and provided checks on the reproducibility of the results [cf. *Mustard and Hays*, 1997].

[18] The UH operates a Nicolet 5SXC FTIR spectrometer capable of providing directional hemispherical reflectance (~3–14 μm, ~3300–715 cm^{-1}) similar to the arrangement of *Salisbury et al.* [1991a, 1994], in which the spectrometer's external port is fitted with an integrating sphere, coated inside with a diffusely reflecting gold surface, and a liquid nitrogen-cooled Hg-Cd-Te (MCT) detector, covering a sample spot size of ~1.5 cm [*Johnson et al.*, 1998]. The spectrometer was configured to provide 8 cm^{-1} resolution with 1000 scans co-added per sample spectrum. Radiance spectra were ratioed to the spectrum of a diffusely reflecting gold plate obtained directly prior to each measurement to provide a reflectance spectrum. To avoid water and CO_2 absorptions at short wavelengths, spectra are presented here from 5 to 14 μm (2000 to 715 cm^{-1}).

[19] Until mid-1999, ASU operated a Mattson Cygnus 100 FTIR spectrometer equipped with an uncooled deuterated triglycine sulphate (DTGS) detector adapted for emission spectroscopy [*Ruff et al.*, 1997]. This instrument was configured to provide 4 cm^{-1} resolution from ~6 to 25 μm (~1670 to 400 cm^{-1}) with 180 interferograms co-added per sample spectrum and was used for the majority of the emission measurements presented here. Additional spectra were obtained using a new Nicolet Nexus 670 spectrometer with optics that extended the wavelength coverage to 50 μm (200 cm^{-1}). This instrument also was configured to provide 4 cm^{-1} resolution with at least 180 interferograms co-added per sample spectrum. The spot size for both instruments was ~1 cm [*Ruff et al.*, 1997]. Because some spectra were more affected by water absorptions shortward of ~7 μm (~1400 cm^{-1}) than others, and because the Mattson Cygnus spectra extended to only 25 μm (400 cm^{-1}), spectra are presented here from ~7 to 25 μm (1400 to 400 cm^{-1}).

[20] For both ASU spectrometers the samples were first heated to 80°C in an oven. That temperature was maintained during spectra

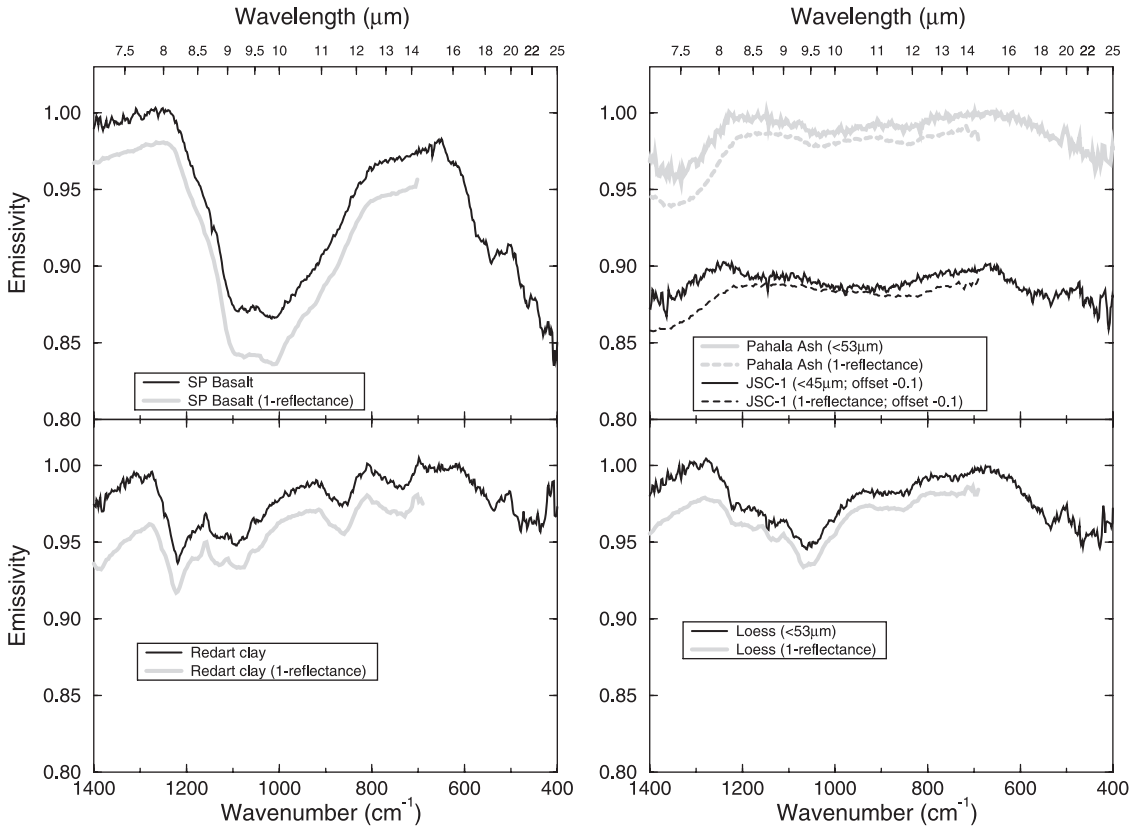

Figure 3. Emission and (1-hemispherical reflectance) spectra of uncoated SP basaltic andesite, Redart clay, Pahala ash, JSC-1 soil, and loess. JSC-1, Pahala ash, and loess were wet-sieved to provide the grain size fraction shown, while Redart grain size is <30 μm. JSC-1 spectra have been offset by −0.1 for clarity. Reflectance spectra are available only to 14 μm (715 cm^{-1}). SiO_2 contents are SP basaltic andesite (57% [*Ulrich*, 1987]), Redart clay (64% [*Smyser*, 1988]), Pahala ash (48% [*Singer*, 1982]), JSC-1 (44% [*Allen et al.*, 1998]), and loess (64% [*Meinert and Busacca*, 2000]).

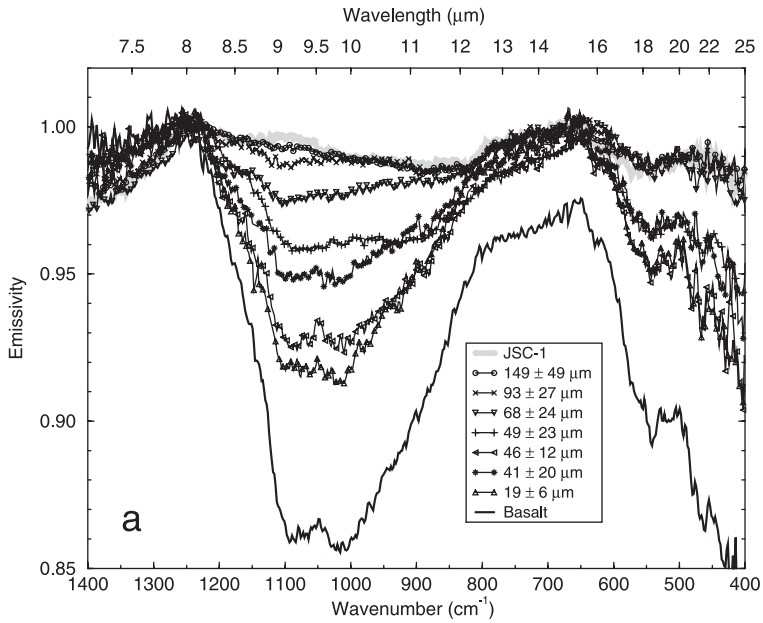

Figure 4. Representative emissivity spectra of the SP basaltic andesite samples coated with (a) JSC-1, (b) Pahala ash, (c) Redart clay, and (d) loess. Measured thicknesses and standard deviations are shown. For clarity, only every third point in the coated sample spectra are symbolized. Note that substantial increases in emissivity occur even with <20 μm coating thickness for all samples in the ∼8–25 μm (1250–400 cm^{-1}) region. Coating thicknesses of ∼100 μm are required to completely obscure the underlying rock for the JSC-1 and Pahala ash, whereas the loess and Redart require only ∼50–65 μm.

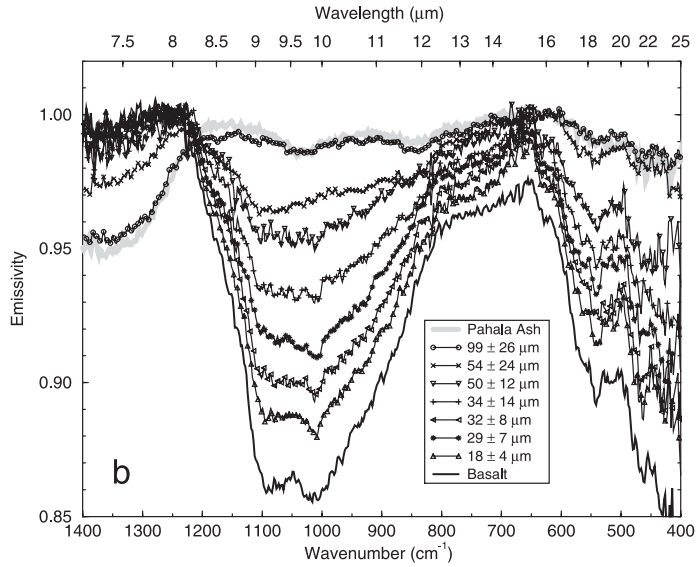

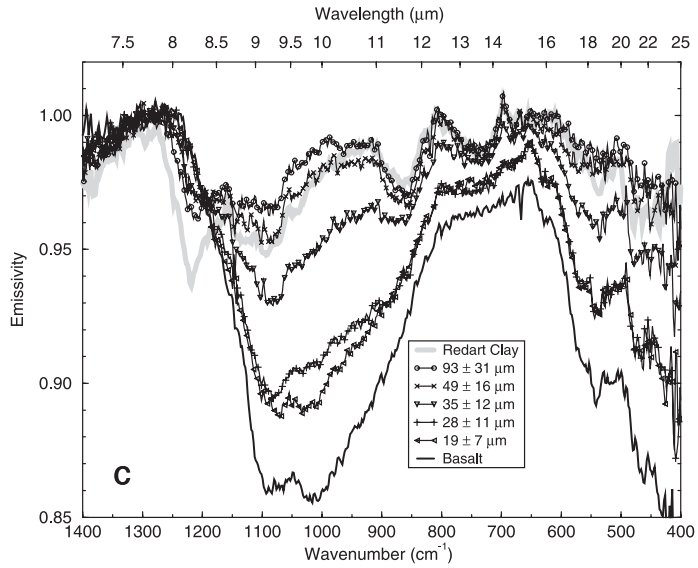

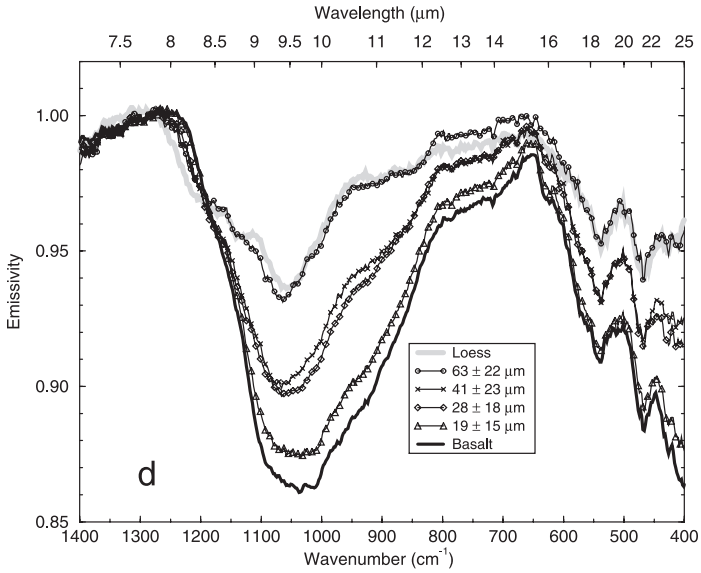

Figure 4. (continued)

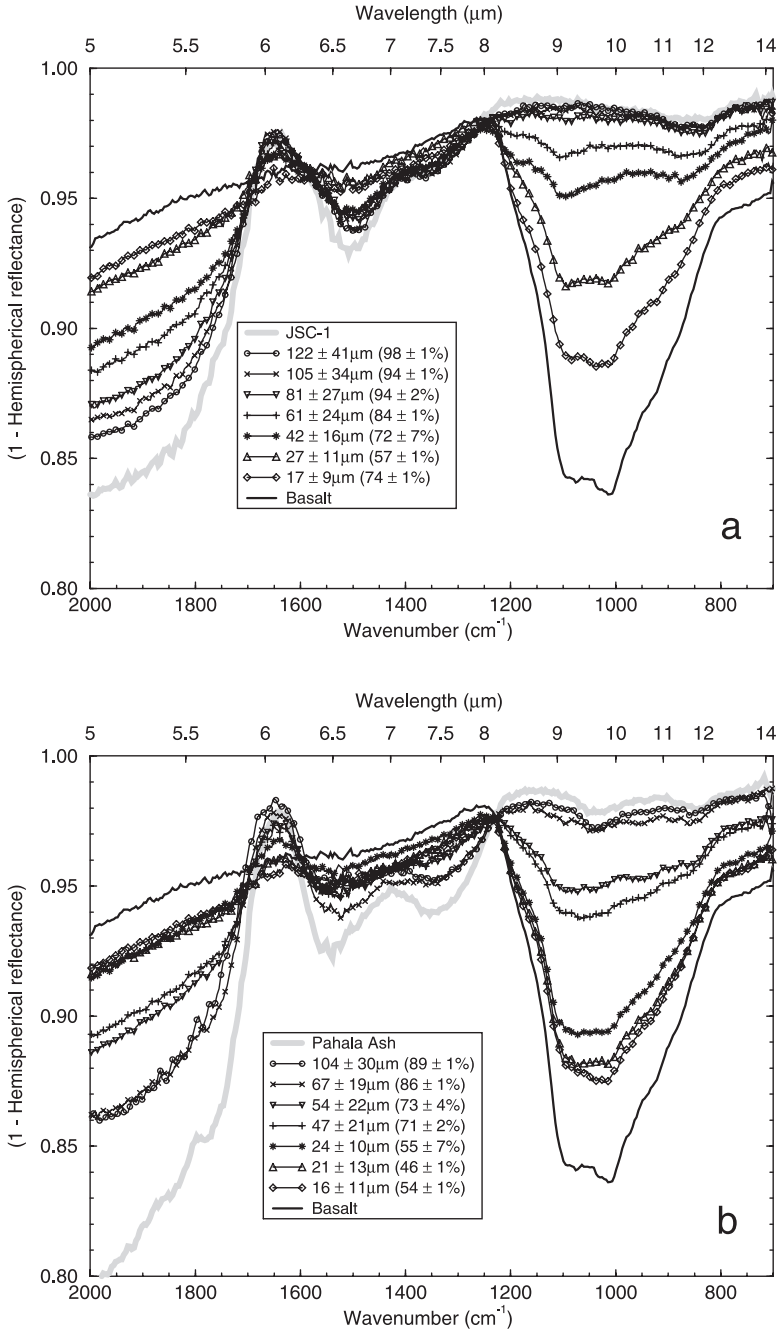

Figure 5. Representative hemispherical reflectance spectra (converted to emissivity) of the SP basaltic andesite samples coated with (a) JSC-1, (b) Pahala ash, (c) Redart clay, and (d) loess. Measured thicknesses and standard deviations are shown, as are average surface area coverage and standard deviation. For clarity, only every third point in the coated sample spectra are symbolized. Note that substantial increases in emissivity occur even with <20 μm coating thickness for all samples in the ~8–25 μm (1250–400 cm^{-1}) region. Coating thicknesses of ~100 μm are required to completely obscure the underlying rock for the JSC-1 and Pahala ash, whereas the loess and Redart require only ~55–75 μm.

acquisition by placing the sample on a heated copper block. Once placed into a Plexiglas glovebox adjacent to the external port of the spectrometer, the energy from the heated sample was collected by a parabolic mirror and directed toward the interferometer. Blackbodies at 70°C and 100°C were used for radiometric calibration. An emissivity spectrum was calculated by dividing the radiance spectrum of the sample by the Planck blackbody radiance spectrum calculated for the maximum brightness temperature, which was computed by assuming that the spectrum had an emissivity equal to 1.0 at some wavelength (usually the Christiansen feature, near 8 μm (1250 cm^{-1}) in these samples) [e.g., *Conel*, 1969; *Ruff et al.*, 1997; *Christensen*, 1998].

4. Results

[21] Figure 3 shows emissivity and reflectance spectra for the uncoated SP basaltic andesite and four of the five coating

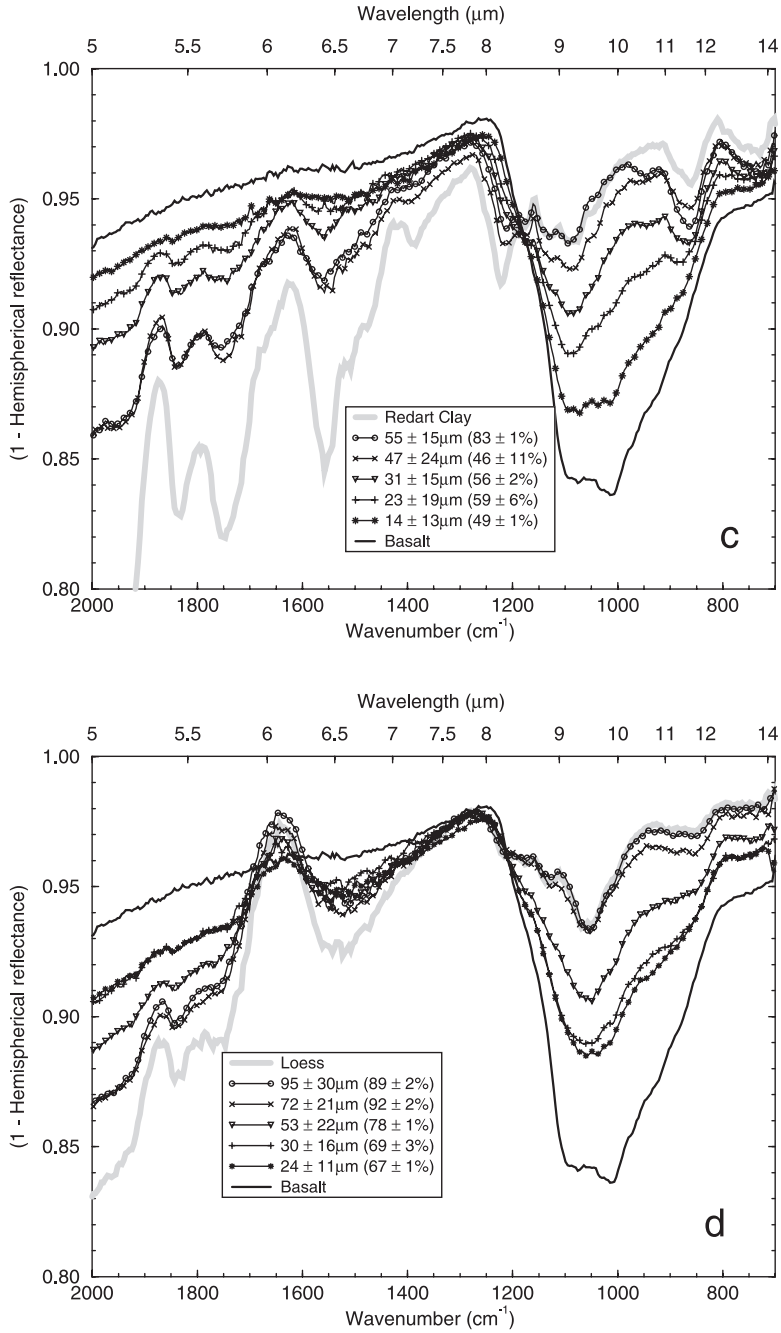

Figure 5. (continued)

materials used in this study. The reflectance spectra were converted to emissivity via Kirchhoff's law (1-hemispherical reflectance [e.g., *Nicodemus*, 1965; *Salisbury et al.*, 1994]). The OM-4 ball clay coated sample spectra are not shown here because of their similarity to Redart clay, although OM-4 spectra were used in the analyses below. The JSC-1 and Pahala ash samples exhibit high emissivity and are nearly spectrally flat between 8 and 18 μm (1250 and 555 cm^{-1}). The Redart clay and loess exhibit spectral features indicative of quartz (~8.5–9.0 μm; ~1175–1110 cm^{-1}), sheet silicates (~9.2–9.6 μm; 1090–1040 cm^{-1}, 18.5–22.2 μm; 540–460 cm^{-1}), and carbonates (~11.2–11.6 μm; 890–860 cm^{-1}). Slight offsets between the emissivity and reflectance spectra result from the requirement that emissivity be equal to 1.0 at some wavelength.

[22] Figure 4 shows representative emissivity spectra (7–25 μm; 1400–400 cm^{-1}) of the SP Flow samples coated with various thicknesses of JSC-1, Pahala ash, Redart clay, and loess. Relative to the dust-free rock, substantial increases in emissivity occur in the ~8–25 μm (1250–400 cm^{-1}) region even at coating thickness <20 μm for all samples. This trend continues with increasing coating thickness until ~100 μm, where the JSC-1 and Pahala ash coatings completely obscure the underlying rock. Thinner coatings (~50–65 μm) of loess and Redart materials obscure the substrate because these materials have more pronounced spectral features than the palagonitic soils. The thickest Redart clay coating (93 μm) exhibits higher emissivity in the 9–10 μm (1100–1000 cm^{-1}) and 20–23 μm (500–430 cm^{-1}) regions than the spectrum of the clay itself. This likely occurs because the clay

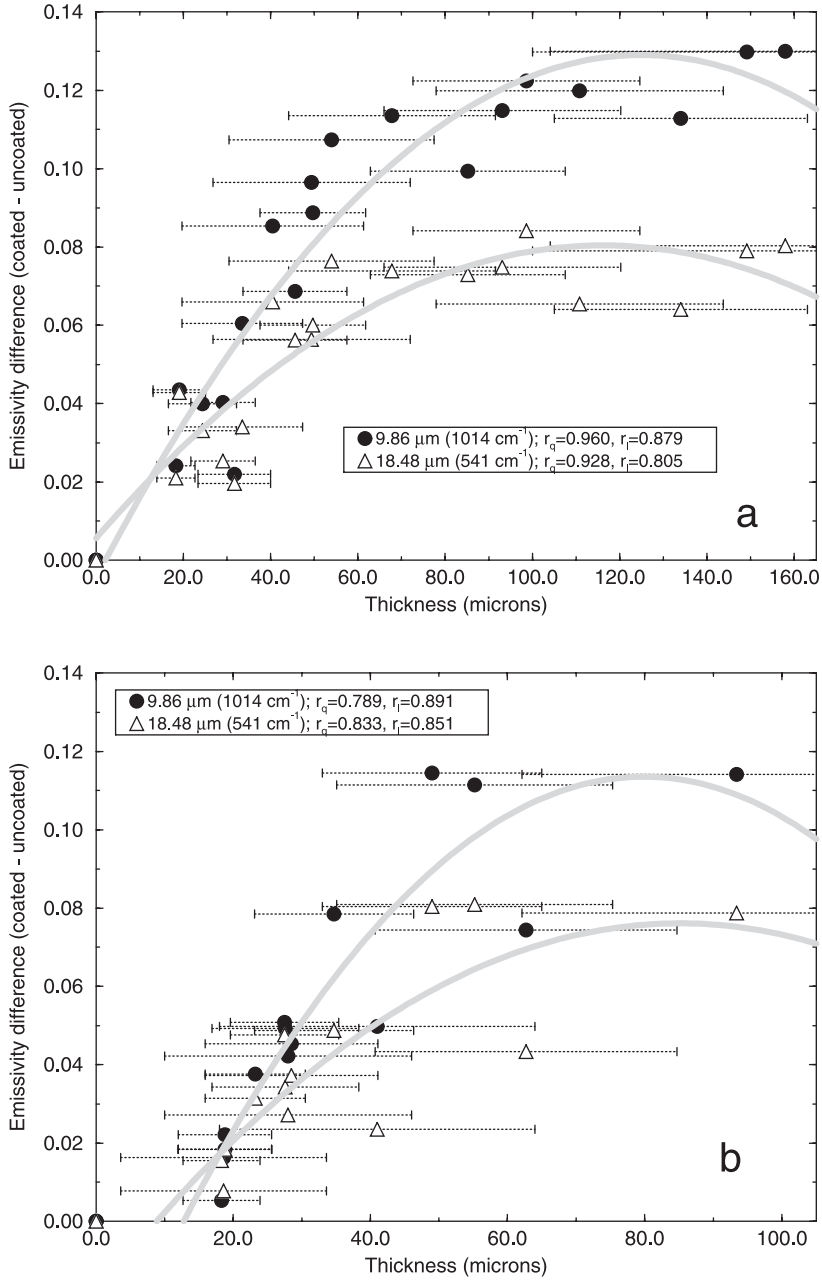

Figure 6. Differences in emissivity between uncoated and coated basaltic andesite samples at two wavelengths for combined (a) JSC-1 and Pahala ash palagonitic coating spectra and (b) Redart and OM-4 ceramic clays and loess coating spectra. Legend shows correlation coefficient for quadratic fit (r_q) and linear fit (r_l) to each data set. Solid curve is quadratic fit to each data set, where the local maximum corresponds to the saturation thickness. Error bars represent standard deviations in thickness measurements for each sample.

powder was slightly compacted during its preparation, which can increase spectral contrast of particulate materials in this spectral region [e.g., *Salisbury et al.*, 1991b]. At wavelengths shorter than ~8 μm (1250 cm^{-1}) (i.e., near the Christiansen feature), emissivity of the coated samples and pure dust is often lower than the basalt, particularly for the Pahala ash spectra. This spectral contrast reversal is observed more clearly in the wavelength region <6 μm (1667 cm^{-1}) afforded by the hemispherical reflectance spectra.

[23] In Figure 5, hemispherical reflectance spectra (5–14 μm; 2000–715 cm^{-1}) converted to emissivity are shown for samples coated with the same materials as Figure 4. Shown alongside the measured thickness for each sample is the estimated areal coverage calculated using digital images as described above. These spectra also demonstrate that the thinnest coatings increase the emissivity of the substrate substantially in the ~8–14 μm (1250–715 cm^{-1}) region and that ~100 μm coatings of JSC-1 and Pahala ash obscure the underlying rock completely. The Redart clay and loess coatings again require only ~55–75 μm thickness to obscure the substrate. However, though the thickest coatings mimic the pure dust spectrum in the ~8–14 μm (1250–715 cm^{-1}) region, they do not at wavelengths less than ~7 μm (1428 cm^{-1}), where the emissivity of the dust spectrum is lower than that of the thickest coatings. Normally, decreased emissivity in this spectral region indicates very small particle sizes [e.g., *Salisbury et al.*, 1991a, 1991b; *Mustard and Hays*, 1997]. It may be that the aggregate particles observed to populate the coated sample surfaces (Figure 2)

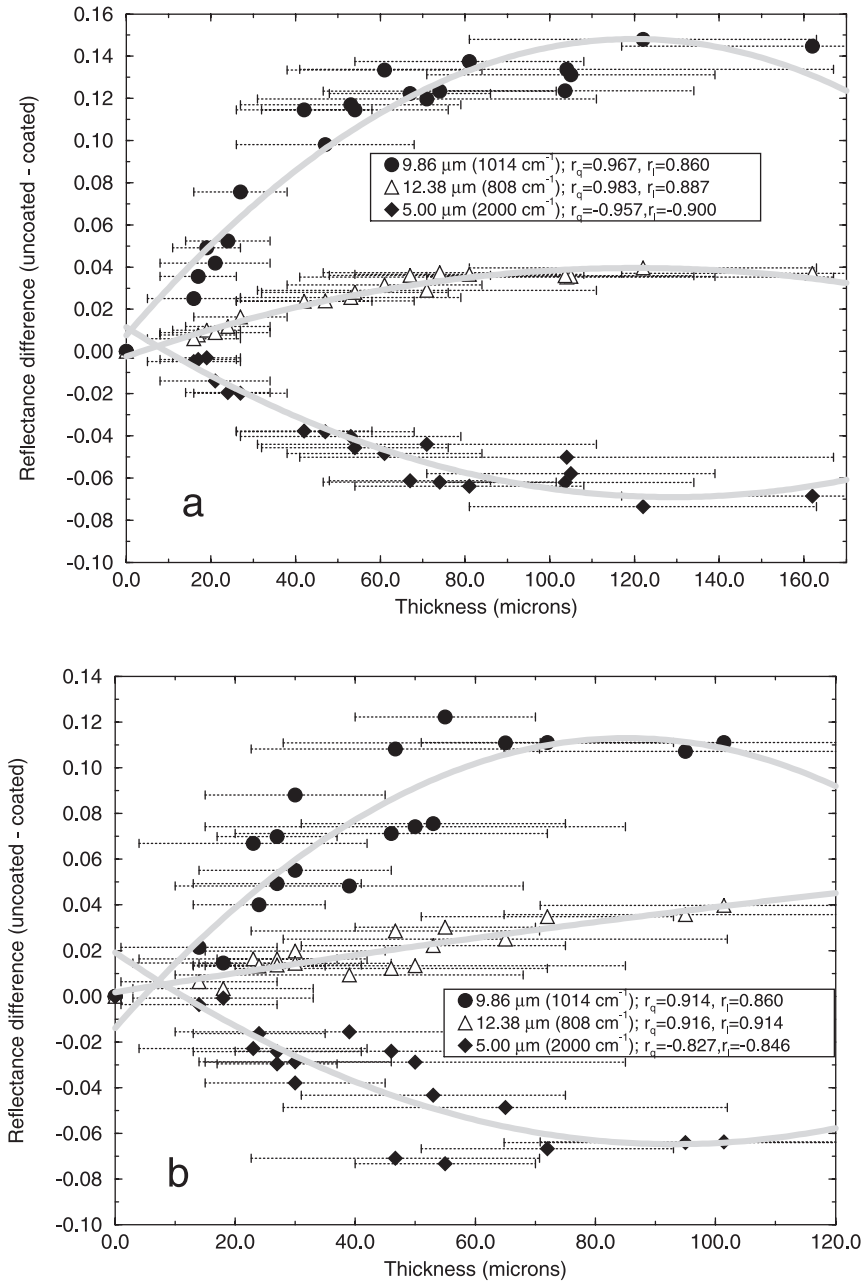

Figure 7. Differences in reflectance between coated and uncoated basaltic andesite samples at three wavelengths for combined (a) JSC-1 and Pahala ash palagonitic coatings and (b) Redart and OM-4 ceramic clays and loess coatings. Legend shows correlation coefficient for quadratic fit (r_q) and linear fit (r_l) to each data set. Solid curve is quadratic fit to each data set, where the local maximum corresponds to the saturation thickness. Error bars represent standard deviations in thickness measurements for each sample.

are sufficiently larger than those in the "pure" dust spectrum itself to cause this effect, although this conflicts with the above notion that the pure dust sample was more compacted than the deposited dust coatings. Alternatively, the residual rock substrate patches still visible to the spectrometer even at thick coatings could cause the observed higher emissivity, although it also appears from the spectra in Figure 5 that even thicker coatings would not necessarily decrease the emissivity to match a given coating material spectrum in this spectral region.

[24] *Crisp and Bartholomew* [1992] found that the biconical reflectance of their palagonite-coated basalts were nearly linearly correlated with exposed surface area of the substrate at several wavelengths. This is consistent with the linear mixing nature of TIR spectra as demonstrated experimentally for mineral mixtures and rocks by several workers [e.g., *Lyon*, 1963, 1964; *Aronson et al.*, 1967; *Thomson and Salisbury*, 1993; *Ramsey and Christensen*, 1998; *Feely and Christensen*, 1999; *Hamilton and Christensen*, 2000]. We also observe that with increasing deposit thickness emissivity linearly increases in the 8–25 μm (1250–400 cm^{-1}) region and linearly decreases in the <8 μm (1250 cm^{-1}) region until the thickness becomes great enough that little further change is observed. We refer to this value as the "saturation thickness," which ranges from ~50–75 μm for the ceramic clay and loess coatings to ~100–120 μm for the palagonitic JSC-1 and Pahala ash coatings.

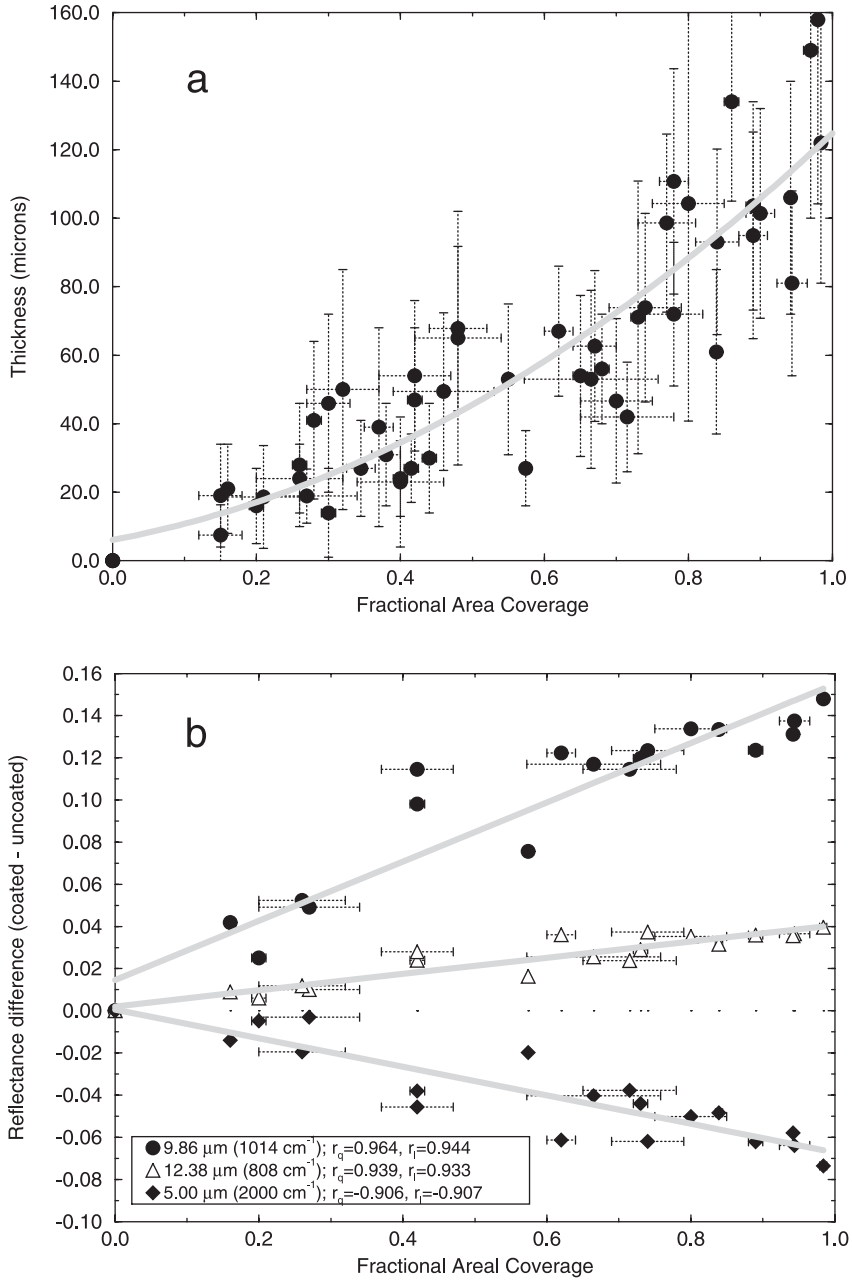

Figure 8. (a) Comparison of measured coating thicknesses and associated standard deviation bars for 50 samples compared to their fractional area coverage computed using digital photomicrographs of each sample (see text). A quadratic fit to the points (solid curve) has a better correlation coefficient (r_q = 0.911) than a linear fit (r_l = 0.893). (b) Differences in reflectance between uncoated and coated samples at three wavelengths for combined JSC-1 and Pahala ash palagonitic coatings compared to fractional area coverage, demonstrating a more linear trend (solid lines) than when compared to coating thickness (Figure 7a). Correlation coefficients for linear (r_l) and quadratic (r_q) fits shown.

[25] Figure 6 illustrates the difference in emissivity between uncoated and coated samples at two wavelengths: the lowest emissivity position in the reststrahlen band at 9.86 μm (1014 cm^{-1}), and one of the longer-wavelength absorptions attributable to pyroxene in the basaltic andesite at 18.48 μm (541 cm^{-1}) [e.g., *Hamilton*, 2000; *Hamilton and Christensen*, 2000; *Ulrich*, 1987]. Although linear fits to these difference values provide good correlation coefficients (r_l values shown in Figure 6), quadratic equations provide better fits (r_q values in Figure 6) for the JSC-1 and Pahala ash coatings because of the additional data available for coatings greater than the saturation thickness. As such, the quadratic fits are overlain in Figure 6 to help emphasize where the emissivity differences reach the saturation thickness (i.e., at the local maximum of the fit). The downturns in the fits after reaching the saturation thickness are a consequence of the quadratic function and do not imply that emissivity differences decrease after that point.

[26] Figure 7 shows reflectance differences between coated and uncoated samples at the 9.86 μm (1014 cm^{-1}) band in addition to the reststrahlen band shoulder at 12.38 μm (808 cm^{-1}) and the

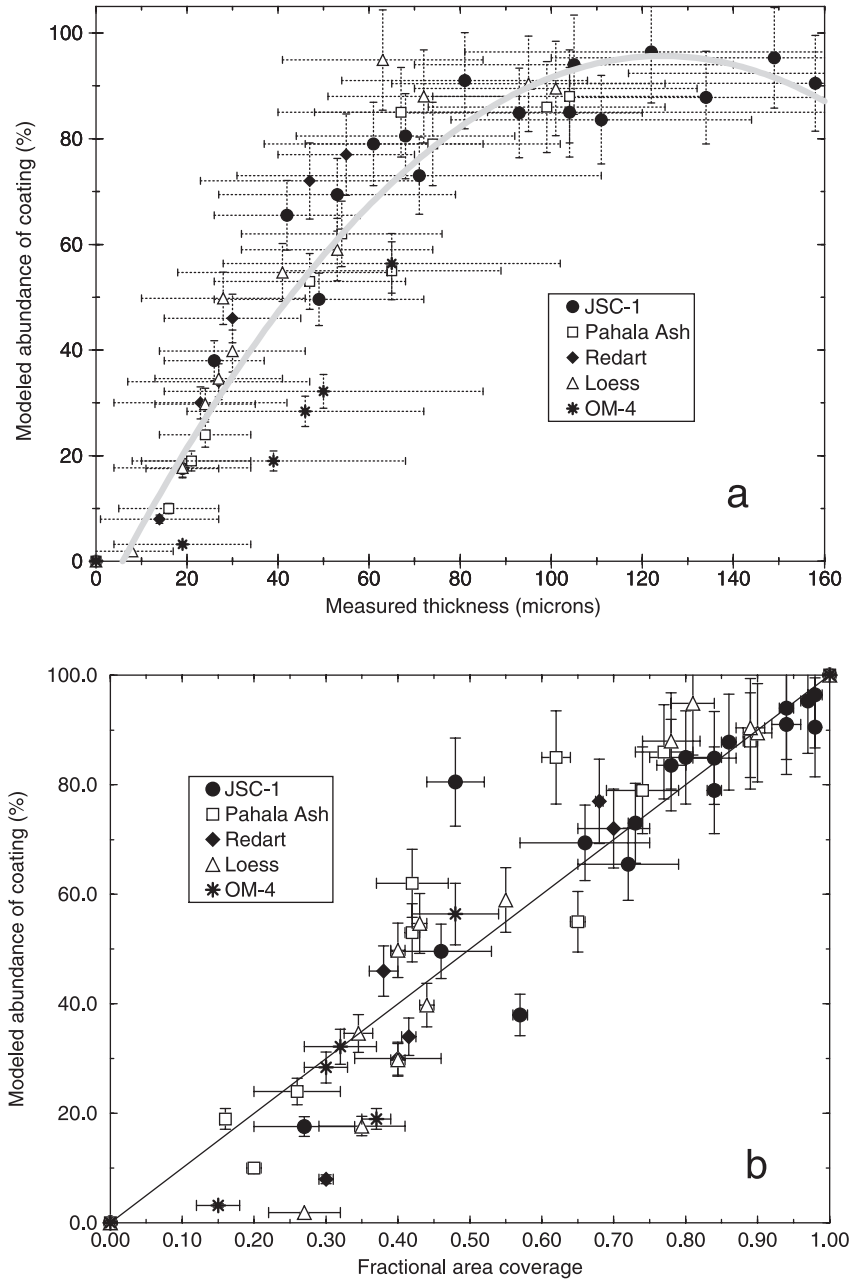

Figure 9. (a) Comparison of measured thickness of coated samples and their modeled coating abundances [cf. *Ramsey and Christensen*, 1998]. Solid curve is quadratic fit to the points, where the local maximum in modeled abundance occurs near the saturation thickness (100–120 μm). Error bars represent standard deviations of measured thicknesses and a 10% uncertainty in the modeled abundance of coating material. (b) Abundances derived from deconvolution model compared to derived fractional area coverage of each sample, with a 1:1 correlation line shown for reference.

shortest-wavelength region at 5.00 μm (2000 cm^{-1}). Here the palagonitic coatings again exhibit better correlations for quadratic fits (Figure 7a) whose local maxima correspond to a saturation thickness near 100–120 μm. The availability of more samples with ceramic clay and loess coatings greater than the saturation thickness results in nearly equal correlations between the linear and quadratic fits (Figure 7b). Although the relatively high emissivity of the 12.38 μm (808 cm^{-1}) shoulder in the uncoated rock provides less dynamic range with which to observe the effects of dust coatings, the overall trend is still discernible in the difference plot. The negative slope of the 5.00 μm (2000 cm^{-1}) region fits results from the contrast reversal relative to the longer-wavelength regions, as discussed above.

[27] The linearity of spectral mixing in the TIR is normally considered a function of surface area coverage by respective model end-members [e.g., *Ramsey and Christensen*, 1998] rather than the thickness of deposited materials. Because air fall deposition of fine-grained particles does not result in equal surface area coverage at the scale of the grains (Figure 2), the relation between areal coverage and deposit thickness should be nonlinear. Figure 8a demonstrates that the correlation between coating thickness and average areal coverage (computed using methods given above) is

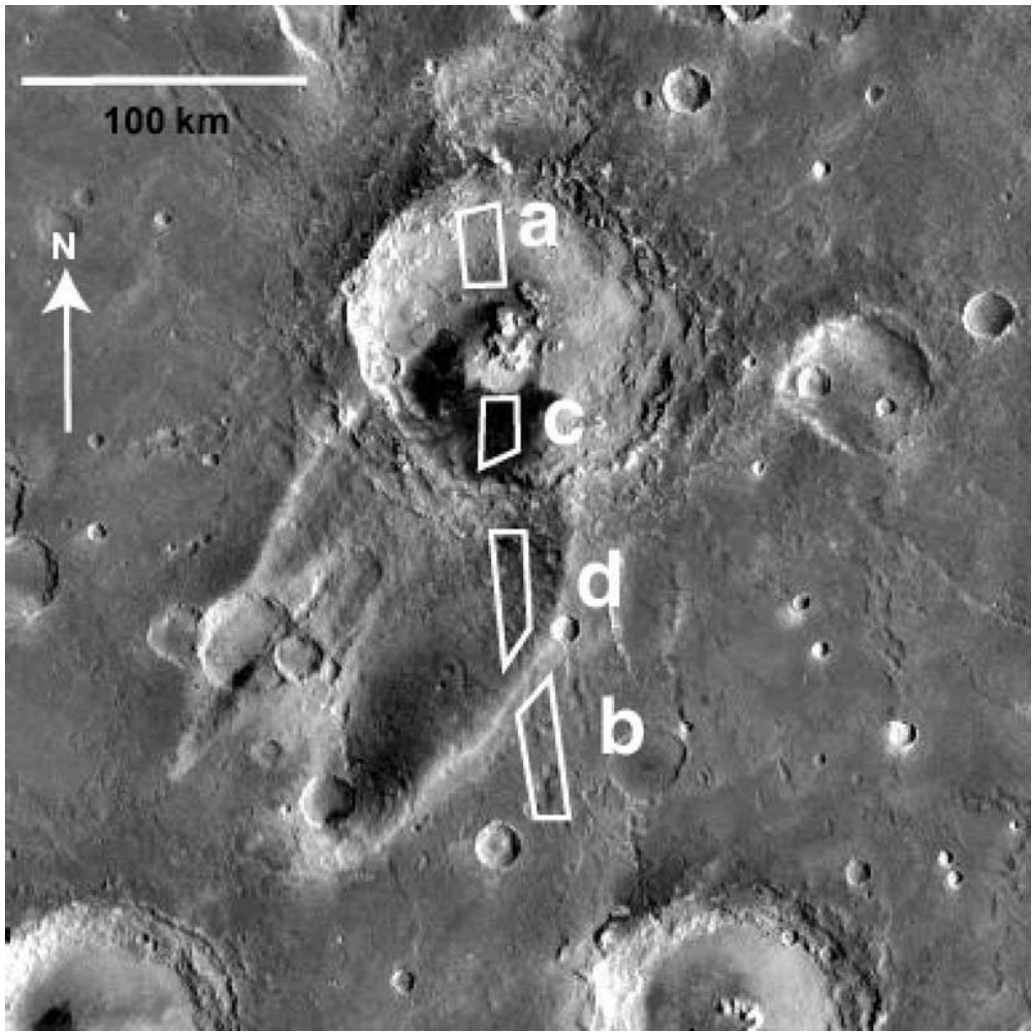

Figure 10. Mars digital image map produced from Viking Orbiter data of Radau crater (17.3°N, 4.7°W; 115 km). Polygons represent the following regions from which TES spectra were acquired on orbit 2795, with TES ICK (time interval) ranges given: (a) bright crater interior, ICKS 1917–1921; (b) plains south of crater, ICKS 1886–1892; (c) dark crater interior, ICKS 1907–1910; (d) dark windtail, ICKS 1896–1902.

indeed nonlinear and can be fit better with a quadratic (r_q = 0.911) than with a linear (r_l = 0.893) function. The lack of data at fractional areas <15% is likely due to small crystals and vesicles on the bare portions of rock substrate which were considered as low-variance regions by the variance operator and thus classified as coating material. When the reflectance differences for the palagonitic soils in Figure 7a are plotted as a function of areal coverage instead of coating thickness, the observed trends become more linear. This is shown in Figure 8b, where the correlation coefficients of linear and quadratic fits are very similar.

[28] An alternative test of the linearity of the coated sample spectra is to use the rock and coating spectra as simple end-members in a spectral deconvolution algorithm. A version of the *Ramsey and Christensen* [1998] model was used to determine the abundances of each end-member for a given coated sample spectrum. The model performs a numerical least squares fit using chi-square minimization to determine the percentage of each end-member fraction, constrained by the requirement that the fractions must sum to unity. In general, the resulting abundances are accurate to within 10–15% uncertainty using this model, depending on the spectral library used and complexity of the input spectrum. In this particular case the input spectra are known to be composed solely of the rock and coating end-members, which lowers the model uncertainty estimates to a few percent.

[29] All spectra of coated samples for which photomicrographs were acquired were run through the deconvolution model for comparison to both the measured thickness and derived areal coverage for each sample. Root-mean-square (RMS) errors on all model runs were <0.01%, and residual error spectra were observed to check for spurious model results. Although the emissivity data obtained shortward of ~7.2 μm (1400 cm^{-1}) are more affected by water absorptions compared to the reflectivity data in this region, it was determined that inclusion of this spectral region did not affect the RMS errors by more than 0.003%. As such, for consistency the 5.0–14.3 μm (2000–700 cm^{-1}) region was used for both reflectance and emissivity spectra here. Figure 9a shows that the measured thicknesses correlate well with the modeled coating abundances until near the saturation thickness (as illustrated by the local maximum of the quadratic fit), at which point a plateau of >90% coating abundance is reached. Figure 9b shows that the modeled abundances compare very well to the estimated fractional area coverage for each coated sample. In particular, samples with dense areal coverage correlate well with the highest modeled coating abundances. Intermediate coverage values (0.35–0.65)

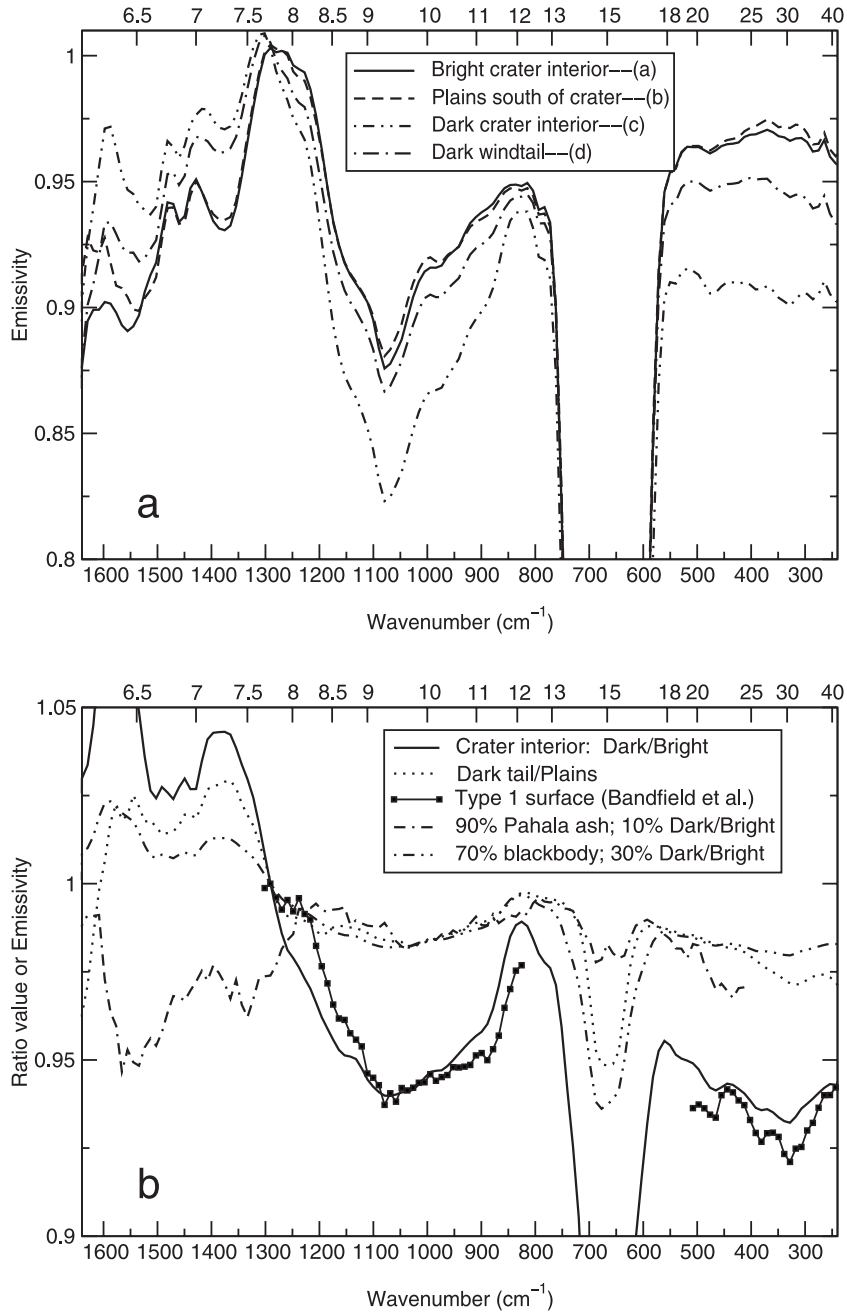

Figure 11. (a) TES emissivity spectra of regions outlined in Figure 10 for Radau crater region. Each spectrum represents an average of n spectra (each smoothed using a 1 × 3 triangular filter) with an average maximum brightness temperature BT: bright crater interior (n = 30; BT = 272°K); dark crater interior (n = 26; BT = 289°K); dark windtail (n = 36; BT = 282°K); plains south of crater (n = 39; BT = 276°K). Data acquired from TES orbit 2795 (L_S = 151°). Note deeper 9.3 μm (1075 cm^{-1}) band for darker materials. (b) Emissivity ratio spectrum of dark/bright crater interior deposits compared to Type 1 Mars surface derived by *Bandfield et al.* [2000a]. Also shown is a ratio spectrum of (dark windtail/bright plains) compared to mixtures of the dark/bright crater interior ratio spectrum plus (1) an emissivity pahala ash spectrum and (2) a blackbody spectrum. See color version of this figure at back of this issue.

are underestimated slightly from a 1:1 correlation line, whereas the lowest areal coverage values (<0.35) are overestimated somewhat. This is an indication of the limitations of the area estimation technique and its dependence on the threshold used on variance images. At sparse coverage the technique is sensitive to smooth (low-variance) regions on the rock substrate in addition to any out of focus grains. At intermediate coverage the technique is dependent on the degree of grain aggregation and shadowing. The result is that the technique's uncertainty is ∼20% at low and intermediate areal coverage (<0.65) but ∼10% at higher values (>0.65).

5. Application to TES

[30] To provide an example of the spectral effects of dust coatings observed in TES spectra, we examined Radau crater (17.3°N, 4.7°W; 115 km), one of the large impact craters in the

Arabia Terra region that exhibits dark intracrater dunes and a dark wind streak associated with bright plains [*Thomas and Veverka*, 1979, *Thomas and Veverka*, 1986; *Christensen*, 1983; *Thomas et al.*, 1981, 1984; *Thomas*, 1984; *Wyatt et al.*, 2001]. All TES mapping phase orbits through orbit 3947 were searched in the Radau region that occurred between $L_s = 0°$ and 200° (to avoid the onset and decay of the dust storm season [e.g., *Martin and Zurek*, 1993]). TES orbit 2795 ($L_s = 151°$) was chosen because it provided data with low dust opacity and low water ice cloud coverage in order to minimize atmospheric contamination [e.g., *Curran et al.*, 1973; *Smith et al.*, 2000; *Pearl et al.*, 2001], and it offered good coverage of the dark and bright interior crater deposits, the dark wind tail, and the nearby plains (Figure 10).

[31] Ideally, emissivity is computed by dividing the calibrated radiance by the Planck function at the kinetic temperature of the surface. For our analyses the surface kinetic temperature was approximated by deriving the brightness temperature from the measured calibrated radiance at each wave number and setting the kinetic temperature equal to the maximum brightness temperature within a wave number internal from 300 to 1350 cm^{-1}. This method assumes that the surface materials have unit emissivity at the point of maximum brightness temperature within this spectral range [*Christensen and Harrison*, 1993; *Ruff et al.*, 1997]; this assumption has been demonstrated to be valid to within ~3% for a wide range of minerals, rocks, and soils [*Salisbury et al.*, 1991b; *Ruff et al.*, 1997]. Each TES calibrated radiance spectrum (~3 × 6 km spatial resolution; 6.1–41.6 μm (1640–240 cm^{-1}) used here) was converted to emissivity in this fashion.

[32] Between 26 and 39 emissivity spectra were averaged for each region using all six TES detectors, and the results are shown in Figure 11a. No compensations were made for the slight differences in band center and spectral resolution among the six detectors [cf. *Christensen et al.*, 2001]. All spectra show deep bands indicative of atmospheric dust (~9.3 μm; 1075 cm^{-1}) and atmospheric CO_2 (e.g., 15 μm; 667 cm^{-1}, hot bands at 12.7 μm; 790 cm^{-1}, 18.2 μm; 550 cm^{-1}). However, there are additional features related to the differences in albedo between the units. For example, the "dust" band is deepest for the dark intracrater materials and shallows successively from the dark windtail to the bright plains. This trend is also observed at longer wavelengths past the main CO_2 band but is reversed at wavelengths <7.5 μm (1333 cm^{-1}). Because this trend is consistent with the spectral effects of dust deposition observed in the laboratory experiments described above, one explanation for this effect could be that the dark intracrater deposits are least contaminated with dust, while the windtail and bright materials are more contaminated.

[33] TES spectra represent complicated mixtures of atmospheric dust, water ice, and surface components that can be rigorously untangled only through the use of radiative transfer and spectral deconvolution techniques [*Christensen et al.*, 1998, 2000a, 2000c, 2001; *Smith et al.*, 2000; *Bandfield et al.*, 2000b]. However, for illustrative purposes, simple ratioing techniques are adequate to investigate the potential effects of dust coatings [e.g., *Pollack et al.*, 1990; *Moersch et al.*, 1997; *Ruff and Christensen*, 1999, 2002]. In this method, spectra from the same orbit and in the same vicinity and elevation are compared under the assumption that the atmospheric constituents do not vary appreciably between the regions of interest. A ratio between two spectra reduces the atmospheric contribution, leaving a combination of the spectral properties of both surfaces plus residual effects due to differences in surface temperature (e.g., CO_2 hot bands [*Maguire*, 1977; *McAfee and Kirkland*, 2000]). However, it is often assumed that the spectra of bright materials exhibit near-unity emissivity (as suggested by the palagonitic soil spectra above [cf. *Christensen et al.*, 2000c]), such that a ratio between very dark and bright materials should provide a first-order estimate of the dark surface spectrum, particularly in the reststrahlen band region (8–14 μm; 1250–715 cm^{-1}). Thus ratios of the dark/bright intracrater deposits and the dark windtail/bright plains spectra can offer further insight into the nature of dust coatings on these surfaces (Figure 11b). The dark/bright intracrater ratio exhibits an overall spectral shape that is very similar to the Type 1 Mars surface (a region in Cimmeria Terra similar to a terrestrial flood basalt) derived by *Bandfield et al.* [2000a]. This implies similar composition, dust coating thickness, and/or dust areal coverage between the dark intracrater deposits and the Type 1 surface. For comparison, the dark windtail/bright plains ratio exhibits reduced spectral contrast consistent with greater dust deposition. We note that a slight difference in the position of the Christiansen features near 7.7 μm (1300 cm^{-1}) between the dark and bright deposits (Figure 11a) may result from differences in composition [e.g., *Conel*, 1969; *Salisbury and Walter*, 1989] or atmospheric absorptions related to brightness temperature differences [e.g., *McAfee and Kirkland*, 2000]. Because these differences are exaggerated in the ratio spectra (Figure 11b), the position of the sharp features near 7.3 μm (1370 cm^{-1}) should not be compared directly to the position of the Christiansen feature in the Type 1 surface spectrum.

[34] If one considers the dark/bright intracrater ratio to represent to first order the emissivity spectrum of the dark materials, a mixture of 10% of this ratio spectrum and 90% of a Pahala ash spectrum (convolved to match the TES sampling of 10 cm^{-1}) matches the windtail/plains ratio spectrum well in the 8–14 μm (1250–715 cm^{-1}) region but less well in the <8 μm (1250 cm^{-1}) and >18 μm (556 cm^{-1}) regions. The poorer fit in these regions could result from particle size differences between the Pahala ash soil and the dust coating the windtail deposit, or slight residual variations in atmospheric dust between the windtail and plains locations.

[35] We also note in Figure 11b that a slightly better fit to the windtail/plains ratio spectrum can be obtained by mixing the dark/bright intracrater ratio spectrum with a simple blackbody spectrum in a 30:70 proportion. This might imply that the differences between the dark and bright materials in the Radau windtail arise dominantly from variations in particle size of the same material, as suggested by *Ruff and Christensen* [1999, 2002] in their studies of dark/bright intracrater materials. The relatively higher emissivity values for the dark deposits in the <8 μm (1250 cm^{-1}) region in Figure 11a also likely are caused by relatively larger particle sizes. The ratio spectra in Figure 11b further demonstrate this effect where the dark/bright material ratio values are highest in the <8 μm (1250 cm^{-1}) region [cf. *Johnson et al.*, 1993].

[36] Constraints on particle sizes for Radau crater materials are available from thermal inertia values derived by combining TES nighttime surface temperature data with daytime albedo measurements [*Pelkey et al.*, 2001; S. Pelkey, personal communication, 2000]. These values (and their corresponding particle size estimates from *Presley and Christensen* [1997]) are ~300–340 J m^{-2} $s^{1/2}$ K^{-1} (~1000 μm) for the dark intracrater deposit, ~190–210 J m^{-2} $s^{1/2}$ K^{-1} (~130 μm) for the bright intracrater materials, ~235–265 J m^{-2} $s^{1/2}$ K^{-1} (~350 μm) for the windtail, and ~135–155 J m^{-2} $s^{1/2}$ K^{-1} (~30 μm) for the southern plains (Figure 10). Similar thermal inertia values are quoted for the deposits associated with the Pettit wind streak by *Christensen et al.* [2001] and *Mellon et al.* [2000]. These data suggest progressively finer particle sizes from the relatively uncoated (dark intracrater material) to nearly completely coated (plains) materials. If the grain sizes derived for the dark intracrater materials and the plains are mixed in the same proportions as the dark materials:blackbody mixture above, the result more closely matches the windtail grain size than does a mixture using the dark materials:Pahala ash proportions. This again suggests that grain size variations may dominate over mineralogical differences between the coated and uncoated materials or that the coating material on Mars is even more spectrally flat (i.e., blackbody-like) than the palagonitic soils studied here. Finally, we note that while the effects of vesicularity can increase

emissivity (and decrease thermal inertia) in a somewhat similar fashion to the effects of coatings [e.g., *Robertson and Peck*, 1974; *Ramsey and Fink*, 1999], it is unlikely that these aeolian, fine-grained, intracrater deposits are highly vesiculated.

6. Conclusions

[37] Important insights to the thermal infrared spectral effects of fine-particle coatings that obscure rock and soil surfaces on Mars have been provided here by systematically combining (1) the techniques of air fall deposition of Mars analog soils and other coatings onto basaltic andesite rock surfaces; (2) microscope measurement of coating thickness; (3) surface area coverage estimation using digital photomicrographs; and (4) acquisition of TIR directional hemispherical reflectance and emission spectra. The spectra acquired here are unlike previous transmission or biconical reflectance spectra of dust coatings [e.g., *Crisp and Bartholomew*, 1992] in that they fully sample the material's thermal radiation, allowing more direct comparison to TIR spectra of Mars. We showed that even very thin coatings (10–20 μm) can reduce the spectral contrast of the main reststrahlen bands (8–14 μm; 1250–715 cm^{-1}) of the rock substrate substantially and superimpose the spectrum of the coating material. This spectral contrast reduction continued in a linear fashion with increasing coating thickness until a saturation thickness was reached, after which little further spectral contrast reduction was observed. Using the shorter wavelength coverage afforded by the hemispherical reflectance spectra, we also showed that this effect occurs in the <6 μm (1667 cm^{-1}) region, albeit reversed from that observed in the >8 μm (1250 cm^{-1}) region (Figure 5). This is a potentially important spectral region not well sampled by TES but where other data sets of Mars are available that could provide additional information on such minerals as carbonates and sulfates [cf. *Erard and Calvin*, 1997].

[38] The saturation thickness varied for different coatings because of the spectral contrast differences observed in the coatings themselves (Figure 3). As such, the saturation thickness of the spectrally flat palagonite coatings (JSC-1, Pahala ash) was ~100–120 μm, whereas that for the higher contrast clay coatings (Redart and OM-4 ceramic clay, terrestrial loess) was only ~50–75 μm. In comparisons of coating thickness versus differences between coated and uncoated samples at several wavelengths, quadratic fits provided better correlation than linear fits (Figures 6 and 7). However, comparison of measured coating thicknesses with estimated surface area coverage using digital photomicrographs was also best fit by a quadratic relation (Figure 8a). As such, when the (coated-uncoated) differences were compared to areal coverage, linear and quadratic fits provided nearly equal correlations (Figure 8b).

[39] The linear nature of mixture modeling in the TIR [e.g., *Ramsey and Christensen*, 1998] provided the means to test the laboratory results by comparing the measured coating thickness and estimated areal coverage of a sample to the modeled areal abundance (Figure 9). Again, the comparison to coating thickness was better fit by a quadratic function, whereas the comparison to coating areal coverage was better fit by a linear function. Moderate scatter in the trends was indicative of the uncertainties of both the thickness and areal coverage estimation techniques.

[40] A comparison of TES data of dark and bright intracrater, windstreak, and plains materials associated with Radau crater (Figure 10) offered an example to study the potential effects of dust deposition as applied to TES data. Even when using TES data uncorrected for atmospheric effects, spectra obtained from the same orbit for locations in close proximity and elevation exhibited spectral contrast patterns consistent with the deposition of dust deposits. A ratio between dark/bright intracrater deposits resulted in a spectrum that matched the basaltic Type 1 Mars surface spectra of *Bandfield et al.* [2000a] relatively well in the reststrahlen region. A ratio between dark windtail and surrounding bright plains resulted in a spectrum with much lower contrast. This latter ratio spectrum was modeled relatively well by an areal combination of either 90% Pahala ash and 10% dark/bright intracrater ratio spectrum or 70% blackbody and 30% dark/bright intracrater ratio spectrum. This suggested that the observed contrast reductions in the windtail deposit could result from either the effects of dust coatings or an overall smaller particle size population than the dark intracrater materials.

[41] The data presented here improve the ability to discern underlying lithologies that would otherwise be obscured by the dust coatings as well as the mineralogical identification of the dust coating components themselves, all of which is relevant to deciphering the geologic, weathering, climate, and possible biotic history of the Martian crust and surficial materials [e.g., *Bell*, 1996; *Farmer and Des Marais*, 1999]. The capability to estimate coating thickness or areal coverage could be useful in tracking and modeling the aeolian erosion and deposition of dust particles on the surface of Mars [e.g., *Thomas and Veverka*, 1979] as well as measurements of dust properties and deposition rates at past and future landing sites [e.g., *Landis and Jenkins*, 2000; *Jenkins et al.*, 1999]. It will also provide relevant constraints for theoretical scattering models of coatings of various thickness on substrates [e.g., *Hapke*, 1993; *Henderson and Jakosky*, 1997]. These data will be useful for improving interpretation and modeling of not only TES spectra but also data from rover simulation field tests [e.g., *Johnson et al.*, 2001] and future TIR instruments such as THEMIS and the mini-TES [*Christensen et al.*, 1999; *Squyres et al.*, 1999].

[42] **Acknowledgments.** The authors thank C. Allen (JSC) for the JSC-1 soil sample, L. Ely (C. Washington Univ.) for the loess sample, D. Bendel (N. Arizona Univ.) for the ceramic clays, K. Horton (Univ. Hawaii) for assistance with the hemispherical reflectance measurements, E. Scott and S. Krot (Univ. Hawaii) for help with photomicrograph image acquisition, V. Hamilton and S. Ruff (Arizona State Univ.) for assistance with the emissivity measurements, M. Ramsey (Univ. Pittsburgh) for the initial loan of his dust deposition apparatus and for use of his UNMIX deconvolution algorithm, N. Forsberg (Hofstra Univ.) for help with acquisition of the SP basaltic andesite sample, F. Grubb (USGS) for assistance with sample coring and preparation, J. Crisp (JPL) for initial advice on dust deposition techniques, and S. Pelkey (LASP) for providing thermal inertia values for Radau crater. T. Titus (USGS) provided significant assistance with use of his "Vampire" software that was used to extract TES emissivity spectra. Helpful reviews were provided by J. Plescia (USGS), T. Titus, and L. Kirkland (LPI). This material is based upon work supported by the National Aeronautics and Space Administration under contract W-19, 443 issued through the Planetary Geology and Geophysics Program.

References

Allen, C. C., R. V. Morris, K. M. Jager, D. C. Golden, D. J. Lindstrom, M. M. Lindstrom, and J. P. Lockwood, Martian regolith simulant JSC Mars-1, *Lunar Planet. Sci.*, *XXIX*, abstract 1690, 1998.

Aronson, J. R., and A. G. Emslie, Spectral reflectance and emittance of particulate materials, 2, Application and results, *Appl. Opt.*, *12*, 2573–2584, 1973.

Aronson, J. R., and A. G. Emslie, Applications of infrared spectroscopy and radiative transfer to earth sciences, in *Infrared and Raman Spectroscopy of Lunar and Terrestrial Minerals*, edited by C. Karr Jr., pp. 143–164, Academic, San Diego, Calif., 1975.

Aronson, J. R., A. G. Emslie, R. V. Allen, and H. G. McLinden, Studies of the middle- and far-infrared spectra of mineral surfaces for application in remote compositional mapping of the Moon and planets, *J. Geophys. Res.*, *72*, 687–703, 1967.

Arvidson, R. E., E. A. Guinness, M. A. Dale-Bannister, J. Adams, M. Smith, P. R. Christensen, and R. B. Singer, Nature and distribution of surficial deposits in Chryse Planitia and vicinity, Mars, *J. Geophys. Res.*, *94*, 1573–1587, 1989a.

Arvidson, R. E., J. L. Gooding, and H. J. Moore, The Martian surface as imaged, sampled, and analyzed by the Viking landers, *Rev. Geophys.*, *27*, 39–60, 1989b.

Bandfield, J. L., V. E. Hamilton, and P. R. Christensen, A global view of

Martian surface compositions from MGS-TES, *Science*, *287*, 1626–1630, 2000a.

Bandfield, J. L., M. D. Smith, and P. R. Christensen, Spectral data set factor analysis and end-member recovery: Application to analysis of Martian atmospheric particulates, *J. Geophys. Res.*, *105*, 9573–9587, 2000b.

Banerjee, S., and M. K. Mazumder, Surface microstructure of powder layers influenced by the forces of deposition and adhesion in electrostatic coating process, *IEEE Trans. Indust. Appl.*, *36*, 46–52, 2000.

Bell, J. F., III, Iron, sulfate, carbonate and hydrated minerals on Mars, in *Mineral Spectroscopy: A Tribute to Roger G. Burns*, edited by M. D. Dyar, C. McCammon, and M. W. Schaefer, *Spec. Pap. 5*, Geochem. Soc., Houston, Tex., 1996.

Bell, J. F., III, et al., Mineralogic and compositional properties of Martian soil and dust: Preliminary results from Mars Pathfinder, *J. Geophys. Res.*, *105*, 1721–1755, 2000.

Blum, J., and G. Wurm, Experiments on sticking, restructuring, and fragmentation of preplanetary dust aggregates, *Icarus*, *143*, 138–146, 2000.

Christensen, P. R., Eolian intracrater deposits on Mars: Physical properties and global distribution, *Icarus*, *56*, 496–518, 1983.

Christensen, P. R., Regional dust deposits on Mars: Physical properties, age, and history, *J. Geophys. Res.*, *91*, 3533–3545, 1986.

Christensen, P. R., Variations in Martian surface composition and cloud occurrence determined from thermal infrared spectroscopy: Analysis of Viking and Mariner 9 data, *J. Geophys. Res.*, *103*, 1733–1746, 1998.

Christensen, P. R., and S. T. Harrison, Thermal infrared emission spectroscopy of natural surfaces: Application to desert varnish coatings on rocks, *J. Geophys. Res.*, *98*, 19,819–19,834, 1993.

Christensen, P. R., et al., Thermal Emission Spectrometer experiment: Mars Observer mission, *J. Geophys. Res.*, *97*, 7719–7734, 1992.

Christensen, P. R., et al., Results from the Mars Global Surveyor Thermal Emission Spectrometer, *Science*, *279*, 1692–1698, 1998.

Christensen, P. R., B. M. Jakosky, H. H. Kieffer, M. C. Malin, H. Y. McSween Jr., K. Nealson, G. Mehall, S. Silverman, and S. Ferry, The thermal emission imaging system (THEMIS) instrument for the Mars 2001 orbiter, *Lunar Planet. Sci.*, *XXX*, abstract 1470, 1999.

Christensen, P. R., et al., Detection of crystalline hematite mineralization on Mars by the Thermal Emission Spectrometer: Evidence for near-surface water, *J. Geophys. Res.*, *105*, 9623–9642, 2000a.

Christensen, P. R., J. L. Bandfield, V. E. Hamilton, D. A. Howard, M. D. Lane, J. L. Piatek, S. W. Ruff, and W. L. Stevanov, A thermal emission spectral library of rock-forming minerals, *J. Geophys. Res.*, *105*, 9735–9739, 2000b.

Christensen, P. R., J. L. Bandfield, M. D. Smith, V. E. Hamilton, and R. N. Clark, Identification of a basaltic component on the Martian surface from Thermal Emission Spectrometer data, *J. Geophys. Res.*, *105*, 9609–9622, 2000c.

Christensen, P. R., et al., The Mars Global Surveyor Thermal Emission Spectrometer experiment: Investigation description and surface science results, *J. Geophys. Res.*, *106*, 23,823–23,871, 2001.

Christy, A. A., Y-Z. Liang, C. Hui, O. M. Kvalheim, and R. A. Velapoldi, Effect of particle size on diffuse reflectance infrared spectra of polystyrene spheres, *Vibrat. Spectrosc.*, *5*, 233–244, 1993.

Clancy, R. T., and S. W. Lee, A new look at dust and clouds in the Mars atmosphere: Analysis of emission-phase-function sequences from global Viking IRTM observations, *Icarus*, *93*, 135–158, 1991.

Conel, J. E., Infrared emissivities of silicates: Experimental results and a cloudy atmosphere model of spectral emission from condensed particulate mediums, *J. Geophys. Res.*, *74*, 1614–1634, 1969.

Cooper, C. D., and J. F. Mustard, Effects of very fine particle size on reflectance spectra of smectite and palagonite soil, *Icarus*, *142*, 557–570, 1999.

Crisp, J. A., The effect of thin coatings of dust or soil on the bulk APXS composition of the underlying rocks at the Pathfinder landing site, *Lunar Planet. Sci., XXIX*, abstract 1962, 1998.

Crisp, J., and M. J. Bartholomew, Mid-infrared spectroscopy of Pahala Ash palagonite and implications for remote sensing studies of Mars, *J. Geophys. Res.*, *97*, 14,691–14,699, 1992.

Curran, R. J., B. J. Conrath, R. A. Hanel, V. G. Kunde, and J. C. Pearl, Mars: Mariner 9 evidence for H_2O ice clouds, *Science*, *182*, 381–383, 1973.

Eby, R. M., R. E. Arvidson, and A. M. Hofmeister, Mars rover rock measurements in dust environments: Lessons from coated rocks in the southwestern United States, *Lunar Planet. Sci.*, *XXIX*, abstract 1695, 1998.

Edgett, K. S., and M. C. Malin, Martian dust raising and surface albedo controls: Thin, dark (and sometimes bright) streaks and dust devils in MGS MOC high resolution images, *Lunar Planet. Sci.*, *XXX*, abstract 1073, 2000.

Emslie, A. G., and J. R. Aronson, Spectral reflectance and emittance of particulate materials, 1, Theory, *Appl. Opt.*, *12*, 2563–2572, 1973.

Erard, S., and W. Calvin, New composite spectra of Mars, 0.4–5.7 μm, *Icarus*, *130*, 449–460, 1997.

Farmer, J. D., and D. J. Des Marais, Exploring for a record of ancient Martian life, *J. Geophys. Res.*, *104*, 26,977–26,995, 1999.

Feely, K. C., and P. R. Christensen, Quantitative compositional analysis using thermal emission spectroscopy: Application to igneous and metamorphic rocks, *J. Geophys. Res.*, *104*, 24,195–24,210, 1999.

Ferguson, D. C., J. C. Kolecki, M. W. Siebert, D. M. Wilt, and J. R. Matijevic, Evidence for Martian electrostatic charging and abrasive wheel wear from the Wheel Abrasion Experiment on the Pathfinder Sojourner rover, *J. Geophys. Res.*, *104*, 8747–8789, 1999.

Fischer, E. M., and C. M. Pieters, The continuum slope of Mars: Bidirectional reflectance investigations and applications to Olympus Mons, *Icarus*, *102*, 185–202, 1993.

Guinness, E. A., R. E. Arvidson, I. H. D. Clark, and M. K. Shepard, Optical scattering properties of terrestrial varnished basalts compared with rocks and soils at the Viking Lander sites, *J. Geophys. Res.*, *102*, 28,687–28,703, 1997.

Haberle, R. M., Modeling the atmospheric structure and dynamics of the Martian atmosphere, in *The Fifth International Conference on Mars* [CD-ROM], *LPI Contrib. 972*, abstract 6018, Lunar and Planet. Inst., Houston, Tex., 1999.

Hamilton, V. E., Thermal infrared emission spectroscopy of the pyroxene mineral series, *J. Geophys. Res.*, *105*, 9701–9716, 2000.

Hamilton, V. E., and P. R. Christensen, Determining the model mineralogy of mafic and ultramafic igneous rocks using thermal emission spectroscopy, *J. Geophys. Res.*, *105*, 9717–9734, 2000.

Hamilton, V. E., R. V. Morris, and P. R. Christensen, Determining the composition of Martian dust and soils using MGS TES: Midinfrared emission spectra of variable-composition palagonites, *Lunar Planet. Sci.*, *XXXII*, abstract 2123, 2001.

Hanel, R., et al., Investigation of the Martian environment by infrared spectroscopy on Mariner 9, *Icarus*, *17*, 423–442, 1972.

Hanel, R. A., B. J. Conrath, D. E. Jennings, and R. E. Samuelson, *Exploration of the Solar System by Infrared Remote Sensing*, 458 pp., Cambridge Univ. Press, New York, 1992.

Hapke, B., *Theory of Reflectance and Emittance Spectroscopy*, 455 pp., Cambridge Univ. Press, New York, 1993.

Henderson, B. G., and B. M. Jakosky, Near-surface thermal gradients and mid-IR emission spectra: A new model including scattering and application to real data, *J. Geophys. Res.*, *102*, 6567–6580, 1997.

Henry, R. L., The transmission of powder films in the infra-red, *J. Opt. Soc. Am.*, *38*, 775–789, 1948.

Hiroi, T., and C. M. Pieters, Modeling the effects of surface roughness and coating on reflectance spectra, *Eos Trans. AGU*, *73*(14), Spring Meet. Suppl., 187, 1992.

Ho, W.-D., and C.-C. M. Ma, Mid-infrared reflectance of silicone resin coating on metal substrates: Effect of polymeric binders' absorption, *Infrared Phys. Tech.*, *38*, 123–131, 1997.

Hunt, G. R., and L. M. Logan, Variation of single particle mid-infrared emission spectrum with particle size, *Appl. Opt.*, *11*, 142–147, 1972.

Hunt, G. R., and R. K. Vincent, The behavior of spectral features in the infrared emission from particulate surfaces of various grain sizes, *J. Geophys. Res.*, *73*, 6039–6046, 1968.

Jähne, B., *Digital Image Processing Concepts, Algorithms, and Scientific Applications*, 383 pp., Springer-Verlag, New York, 1995.

Jenkins, P. P., G. L. Landis, M. J. Krasowski, D. M. Wilt, L. C. Greer III, J. Lekki, C. R. Baraona, and D. A. Scheiman, Status of the dust accumulation and removal technology experiment for the Mars 2001 Surveyor lander, in *The Fifth International Conference on Mars* [CD-ROM], *LPI Contrib. 972*, abstract 6203, Lunar and Planet. Inst., Houston, Tex., 1999.

Johnson, J. R., and W. M. Grundy, Visible/near-infrared spectra and two-layer modeling of palagonite-coated basalts, *Geophys. Res. Lett*, *28*, 2101–2104, 2001.

Johnson, J. R., P. G. Lucey, K. A. Horton, and E. M. Winter, Infrared measurements of pristine and disturbed soils, 1, Spectral contrast differences between field and laboratory data, *Remote Sens. Environ.*, *64*, 34–46, 1998.

Johnson, J. R., et al., Geological characterization of remote field sites using visible and infrared spectroscopy: Results from the 1999 Marsokhod field test, *J. Geophys. Res.*, *106*, 7683–7711, 2001.

Johnson, P. E., K. J. Vogler, and J. P. Gardner, The effect of surface roughness on lunar thermal emission spectra, *J. Geophys. Res.*, *98*, 20,825–20,829, 1993.

Kieffer, H. H., T. N. Titus, K. F. Mullins, and P. R. Christensen, Mars south polar spring and summer behavior observed by TES: Seasonal cap evolution controlled by frost grain size, *J. Geophys. Res.*, *105*, 9653–9700, 2000.

Landis, G. A., and P. P. Jenkins, Measurement of the settling rate of atmo-

spheric dust on Mars by the MAE instrument on Mars Pathfinder, *J. Geophys. Res.*, *105*, 1855–1858, 2000.
Lindstrom, I. K., and M. M. Lindstrom, The effect of "Martian" dust on the reflectance spectra of igneous and sedimentary rocks, *Lunar Planet. Sci.*, *XXIX*, abstract 1886, 1998.
Lyon, R. J. P., Evaluation of infrared spectrophotometry for compositional analysis of lunar and planetary soils, *NASA Tech. Note, NASA TN-D-1871*, 1963.
Lyon, R. J. P., Evaluation of infrared spectrophotometry for compositional analysis of lunar and planetary soils, Part 2, *NASA CR-100*, 1964.
Maguire, W. C., Martian isotopic ratios and upper limits for possible minor constituents as derived from Mariner 9 infrared spectrometer data, *Icarus*, *32*, 85–97, 1977.
Martin, L. J., and R. W. Zurek, An analysis of the history of dust activity on Mars, *J. Geophys. Res.*, *98*, 3221–3246, 1993.
McAfee, J. M., and L. E. Kirkland, A model-independent correction of Mars thermal spectra near 7.8 μm for $CO^{16}O^{17}$ atmospheric absorption, *Lunar Planet. Sci.*, *XXXI*, abstract 1967, 2000.
McSween, H. Y., Jr., et al., Chemical, multispectral, and textural constraints on the composition and origin of rocks at the Mars Pathfinder landing site, *J. Geophys. Res.*, *104*, 8679–8715, 1999.
Meinert, L. D., and A. J. Busacca, Geology and wine 3: Terroirs of the Walla Walla Valley appellation, southeastern Washington state, USA, *Geosci. Can.*, *27*, 149–171, 2000.
Mellon, M. T., B. M. Jakosky, H. H. Kieffer, and P. R. Christensen, High resolution thermal inertia mapping from the Mars Global Surveyor Thermal Emission Spectrometer, *Icarus*, *148*, 437–455, 2000.
Metzger, S. M., J. R. Carr, J. R. Johnson, T. J. Parker, and M. Lemmon, Dust devil vortices seen by the Mars Pathfinder camera, *Geophys. Res. Lett.*, *26*, 2781–2784, 1999.
Moersch, J. E., and P. R. Christensen, Thermal emission from particulate surfaces: A comparison of scattering models with measured spectra, *J. Geophys. Res.*, *100*, 7465–7477, 1995.
Moersch, J. E., T. L. Hayward, P. D. Nicholson, S. W. Squyres, and J. Van Cleve, Identification of a 10-micron silicate absorption feature in the Acidalia region of Mars, *Icarus*, *126*, 183–196, 1997.
Moore, H. J., D. B. Bickler, J. A. Crisp, H. J. Eisen, J. A. Gensler, A. F. C. Haldemann, J. R. Matijevic, L. K. Reid, and F. Pavlics, Soil-like deposits observed by Sojourner, the Pathfinder rover, *J. Geophys. Res.*, *104*, 8729–8746, 1999.
Mustard, J. F., and J. E. Hays, Effects of hyperfine-particles on reflectance spectra from 0.3 to 25 μm, *Icarus*, *125*, 145–163, 1997.
Mustard, J. F., and J. M. Sunshine, Seeing through the dust: Martian crustal heterogeneity and links to the SNC meteorites, *Science*, *267*, 1623–1626, 1995.
Nicodemus, F. E., Directional reflectance and emissivity of an opaque surface, *Appl. Opt.*, *4*, 767–774, 1965.
Pearl, J. C., M. D. Smith, B. J. Conrath, J. L. Bandfield, and P. R. Christensen, Observations of Martian ice clouds by the Mars Global Surveyor Thermal Emission Spectrometer: The first Martian year, *J. Geophys. Res.*, *106*, 12,325–12,338, 2001.
Pecharroman, C., and J. E. Igelsias, Modeling particle size and clumping effects in the IR absorbance spectra of dilute powders, *Appl. Spectrosc.*, *50*, 1553–1562, 1996.
Pelkey, S. M., B. M. Jakosky, and M. T. Mellon, Thermal inertia of crater-related wind streaks on Mars, *J. Geophys. Res.*, *106*, 23,909–23,920, 2001.
Pollack, J. B., T. Roush, F. Witteborn, J. Bregman, D. Wooden, C. Stoker, O. B. Toon, D. Rank, B. Dalton, and R. Freedman, Thermal emission spectra of Mars (5.4–10.5 μm): Evidence for sulfates, carbonates, and hydrates, *J. Geophys. Res.*, *95*, 14,595–14,627, 1990.
Presley, M. A., and P. R. Christensen, Thermal conductivity measurements of particular materials, 2, Results, *J. Geophys. Res.*, *102*, 6551–6566, 1997.
Rafkin, S. C. R., R. M. Haberle, and T. I. Michaels, The Mars regional atmospheric modeling system: Model description and selected simulations, *Icarus*, *151*, 228–256, 2001.
Ramsey, M. S., and P. R. Christensen, Mineral abundance determination: Quantitative deconvolution of thermal emission spectra, *J. Geophys. Res.*, *103*, 577–596, 1998.
Ramsey, M. S., and J. H. Fink, Estimating silicic lava vesicularity with thermal remote sensing: A new technique for volcanic mapping and monitoring, *Bull. Volcanol.*, *61*, 32–39, 1999.
Ramsey, M. S., and N. Lancaster, Using remote sensing to derive sediment mixing patterns in arid environments: Future global possibilities with the ASTER instrument, *Geol. Soc. Am. Abstr. Programs*, *30*, 360, 1998.
Rieder, R., T. Economous, H. Wanke, A. Turkevich, J. Crisp, J. Bruckner, G. Dreibus, and H. Y. McSween Jr., The chemical composition of Martian soil and rocks returned by the mobile Alpha Proton X-Ray spectrometer: Preliminary results from the X-ray mode, *Science*, *278*, 1771–1774, 1997.
Rivard, B., S. B. Petroy, and J. R. Miller, Measured effects of desert varnish on the mid-infrared spectra of weathered rocks as aid to TIMS imagery interpretation, *IEEE Trans. Geosci. Remote Sens.*, *31*, 284–291, 1993.
Robertson, E. C., and D. L. Peck, Thermal conductivity of vesicular basalt from Hawaii, *J. Geophys. Res.*, *79*, 4875–4888, 1974.
Roush, T. L., Effects of iron-silica gels on spectral reflectance, *Lunar Planet. Sci.*, *XIII*, 661–662, 1982.
Roush, T. L., and J. F. Bell III, Thermal emission measurements (5–25 μm) of Hawaiian palagonitic soils with implications for Mars, *Lunar Planet. Sci.*, *XXV*, 1161–1162, 1994.
Roush, T. L., and J. B. Orenberg, Thermal emission measurements (5–25 μm) of palagonite/Fe-substitude montmorillonite intimate mixtures: Applications to Mars, *Lunar Planet. Sci.*, *XXV*, 1163–1164, 1994.
Roush, T. L., J. Pollack, and J. Oreneberg, Derivation of midinfrared (5–25 μm) optical constants of some silicates and palagonite, *Icarus*, 191–208, 1991.
Roush, T. L., J. F. Bell III, and R. V. Morris, Transmission measurements (4000–400 cm^{-1}, 2.5–25 μm) of crystalline ferric oxides and ferric oxyhydroxides: Implications for Mars, *Lunar Planet. Sci.*, *XXV*, 1165–1166, 1994.
Ruff, S. W., and P. R. Christensen, Thermal-infrared spectra characteristics of Martian albedo features: Clues to composition, in *The Fifth International Conference on Mars* [CD-ROM], *LPI Contrib. 972*, abstract 6230, Lunar and Planet. Inst., Houston, Tex., 1999.
Ruff, S. W., and P. R. Christensen, Bright and dark regions on Mars: Particle size and mineralogical characteristics based on Thermal Emission Spectrometer data, *J. Geophys. Res.*, *107*, 10.1029/2001JE001580, in press, 2002.
Ruff, S. W., P. R. Christensen, P. W. Barbera, and D. L. Anderson, Quantitative thermal emission spectroscopy of minerals: A laboratory technique for measurement and collection, *J. Geophys. Res.*, *102*, 14,899–14,913, 1997.
Salisbury, J. W., Mid-infrared spectroscopy: Laboratory data, in *Remote Geochemical Analysis*, edited by C. Pieters and P. Englert, chap. 4, pp. 7–98, Cambridge Univ. Press, New York, 1993.
Salisbury, J. W., and A. Wald, The role of volume scattering in reducing spectral contrast of reststrahlen bands in spectra of powdered minerals, *Icarus*, *96*, 121–128, 1992.
Salisbury, J. W., and L. S. Walter, Thermal infrared (2.5–13.5 μm) spectroscopic remote sensing of igneous rock types on particulate planetary surfaces, *J. Geophys. Res.*, *94*, 9192–9202, 1989.
Salisbury, J. W., B. Hapke, and J. W. Eastes, Usefulness of weak bands in midinfrared remote sensing of particulate planetary surfaces, *J. Geophys. Res.*, *92*, 702–710, 1987.
Salisbury, J. W., D. M. D'Aria, and E. Jarosewich, Midinfrared (2.5–13.5 μm) reflectance spectra of powdered stony meteorites, *Icarus*, *92*, 280–297, 1991a.
Salisbury, J. W., L. S. Walter, N. Vergo, and D. M. D'Aria, *Infrared (2.1–25 μm) Spectra of Minerals*, 267 pp., Johns Hopkins Univ. Press, Baltimore, Md., 1991b.
Salisbury, J. W., A. Wald, and D. M. D'Aria, Thermal-infrared remote sensing and Kirchhoff's law, 1, Laboratory measurements, *J. Geophys. Res.*, *99*, 11,897–11,911, 1994.
Salisbury, J. W., A. Basu, and E. M. Fischer, Thermal infrared spectra of lunar soils, *Icarus*, *130*, 125–139, 1997.
Shelfer, T. D., and R. V. Morris, Effect of a ferric weathering rind on the optical and Mossbauer spectra of a basaltic rock, *Lunar Planet. Sci.*, *XXIX*, abstract 1327, 1998.
Shepard, M. K., and R. E. Arvidson, The opposition surge and photopolarimetry of fresh and coated basalts, *Icarus*, *141*, 172–178, 1999.
Singer, R. B., Spectral evidence for the mineralogy of high-albedo soils and dust on Mars, *J. Geophys. Res.*, *87*, 10,159–10,168, 1982.
Singer, R. B., and P. L. Blake, Effects of mineral grain size and physical particle size on spectral reflectance of basalts, *Lunar Planet. Sci.*, *XIV*, 706–707, 1983.
Singer, R. B., and T. L. Roush, Spectral reflectance properties of particulate weathered coatings on rocks: Laboratory modeling and applicability to Mars, *Lunar Planet. Sci.*, *XIV*, 708–709, 1983.
Sinton, W. M., and J. Strong, Radiometric observations of Mars, *Astrophys. J.*, *131*, 459–469, 1960.
Smith, M. D., J. L. Bandfield, and P. R. Christensen, Separation of atmospheric and surface spectral features in Mars Global Surveyor Thermal Emission Spectrometer (TES) spectra, *J. Geophys. Res.*, *105*, 9589–9607, 2000.
Smith, P. H., et al., Results from the Mars Pathfinder Camera, *Science*, *278*, 1758–1765, 1997.
Smyser, M., An Albany substitute, *Ceramics Mon.*, *36*, 49, 1988.

Squyres, S. W., et al., The Mars 2001 Athena precursor experiment (APEX), *Lunar Planet. Sci.*, *XXX*, abstract 1672, 1999.

Sullivan, R., K. Edgett, M. Malin, P. Thomas, and J. Veverka, Mass-wasting slope streaks imaged by the Mars Orbiter camera, *Lunar Planet. Sci.*, *XXXI*, abstract 1911, 2000.

Thomas, P., Martian intracrater splotches: Occurrence, morphology and colors, *Icarus*, *57*, 205–227, 1984.

Thomas, P., and J. Veverka, Seasonal and secular variation of wind streaks on Mars: An analysis of Mariner 9 and Viking data, *J. Geophys. Res.*, *84*, 8131–8146, 1979.

Thomas, P., and J. Veverka, Red/Violet contrast reversal on Mars: Significance for eolian sediments, *Icarus*, *66*, 39–55, 1986.

Thomas, P. C., J. Veverka, S. Lee, and A. Bloom, Classification of wind streaks on Mars, *Icarus*, *45*, 125–153, 1981.

Thomas, P. C., J. Veverka, D. Gineris, and L. Wong, "Dust" streaks on Mars, *Icarus*, *60*, 161–179, 1984.

Thomson, J., and J. Salisbury, The mid-infrared reflectance of mineral mixtures (7–14 μm), *Remote Sens. Environ.*, *45*, 1–13, 1993.

Tomasko, M. G., L. R. Doose, M. T. Lemmon, P. H. Smith, and E. Wegryn, Properties of dust in the Martian atmosphere from the imager on Mars Pathfinder, *J. Geophys. Res.*, *104*, 8987–9008, 1999.

Ulrich, G. E., SP Mountain cinder cone and lava flow, northern Arizona, in *Centennial Field Guide*, vol. 2, *Rocky Mountain Section of the Geological Society of America*, pp. 385–388, Geol. Soc. of Am., Boulder, Colo., 1987.

Van Tassel, R. A., and J. W. Salisbury, The composition of the Martian surface, *Icarus*, *3*, 264–269, 1964.

Wells, E. N., J. Veverka, and P. Thomas, Mars: Experimental study of albedo changes caused by dust fallout, *Icarus*, *58*, 331–338, 1984.

White, B. R., B. M. Lacchia, R. Greeley, and R. N. Leach, Aeolian behavior of dust in a simulated Martian environment, *J. Geophys. Res.*, *102*, 25,629–25,640, 1997.

Wyatt, M. B., J. L. Bandfield, H. Y. McSween Jr., and P. R. Christensen, Compositions of low albedo intracrater materials and wind streaks on Mars: Examination of MGS TES data in western Arabia Terra, *Lunar Planet. Sci.*, *XXXII*, abstract 1872, 2001.

Xu, W., and S. C. Shen, Infrared radiation and reflection in an inhomogeneous coating layer on an substrate, *Appl. Opt.*, *31*, 4488–4496, 1992.

Younis, M. T., M. A. Gilabert, J. Melia, and J. Bastida, Weathering process effects on spectral reflectance of rocks in a semi-arid environment, *Int. J. Remote Sens.*, *18*, 3361–3377, 1997.

P. R. Christensen, Department of Geology, Arizona State University, Campus Box 871404, Tempe, AZ 85287-1404, USA. (phil.christensen@asu.edu)

J. R. Johnson, Branch of Astrogeology, U.S. Geological Survey, 2255 North Gemini Drive, Flagstaff, AZ 86001, USA. (jrjohnson@usgs.gov)

P. G. Lucey, Hawaii Institute for Geology and Planetology, University of Hawaii at Manoa, 2525 Correa Road, Honolulu, HI 96822, USA. (lucey@higp.hawaii.edu)

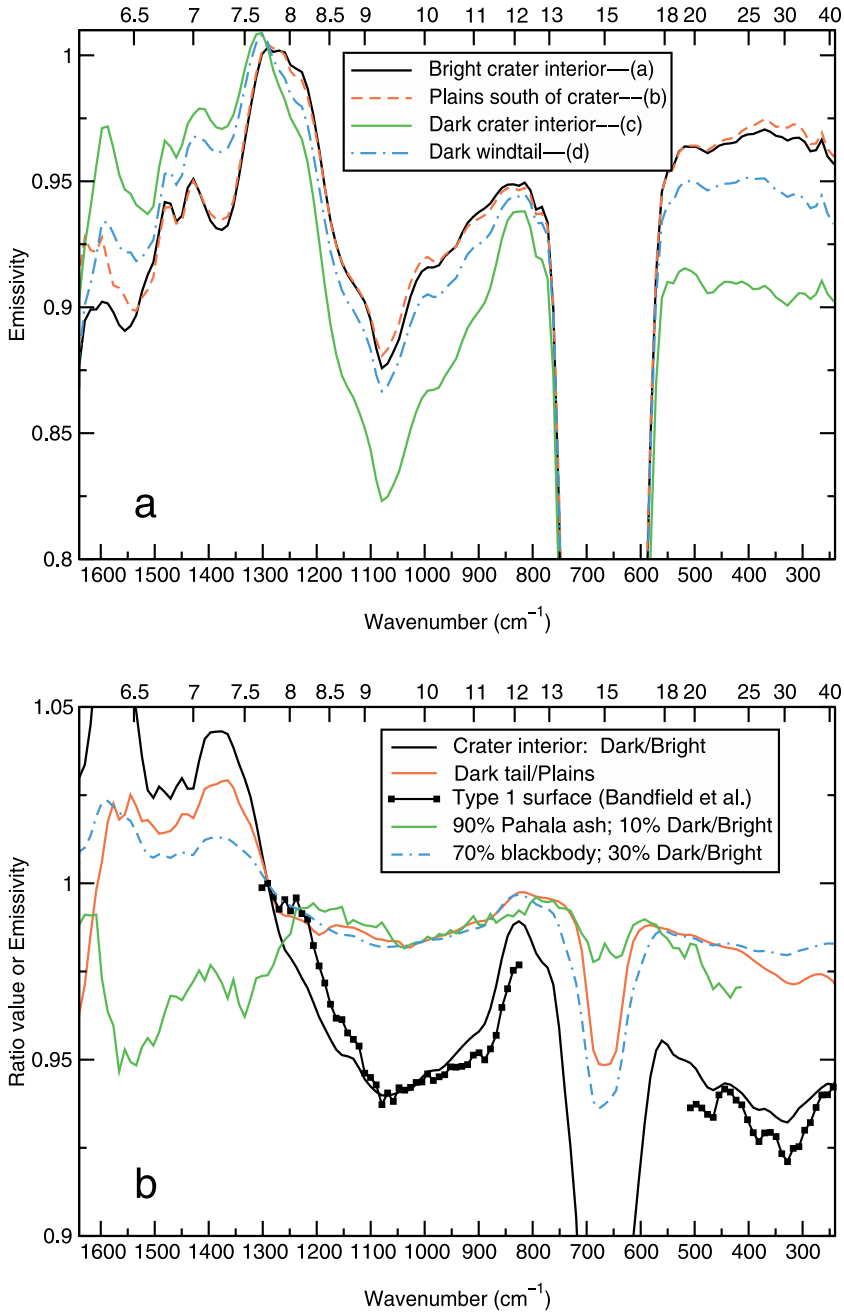

Figure 11. (a) TES emissivity spectra of regions outlined in Figure 10 for Radau crater region. Each spectrum represents an average of n spectra (each smoothed using a 1 × 3 triangular filter) with an average maximum brightness temperature BT: bright crater interior (n = 30; BT = 272°K); dark crater interior (n = 26; BT = 289°K); dark windtail (n = 36; BT = 282°K); plains south of crater (n = 39; BT = 276°K). Data acquired from TES orbit 2795 (L_S = 151°). Note deeper 9.3 μm (1075 cm^{-1}) band for darker materials. (b) Emissivity ratio spectrum of dark/bright crater interior deposits compared to Type 1 Mars surface derived by *Bandfield et al.* [2000a]. Also shown is a ratio spectrum of (dark windtail/bright plains) compared to mixtures of the dark/bright crater interior ratio spectrum plus (1) an emissivity pahala ash spectrum and (2) a blackbody spectrum.